LBL-15590
Preprint c.2

Lawrence Berkeley Laboratory

UNIVERSITY OF CALIFORNIA

Physics, Computer Science & Mathematics Division

RECEIVED
LAWRENCE
BERKELEY LABORATORY

MAY 17 1983

LIBRARY AND
DOCUMENTS SECTION

Submitted for publication

LONGITUDINAL STABILITY OF A COASTING BEAM IN A RESISTIVE VACUUM CHAMBER WITH CYLINDRICAL RESONANT CAVITY. PART II: GRAPHS AND A FORMULA FOR THE COUPLING IMPEDANCE

Robert L. Warnock and George R. Bart

February 1983

TWO-WEEK LOAN COPY

This is a Library Circulating Copy which may be borrowed for two weeks. For a personal retention copy, call Tech. Info. Division, Ext. 6782.

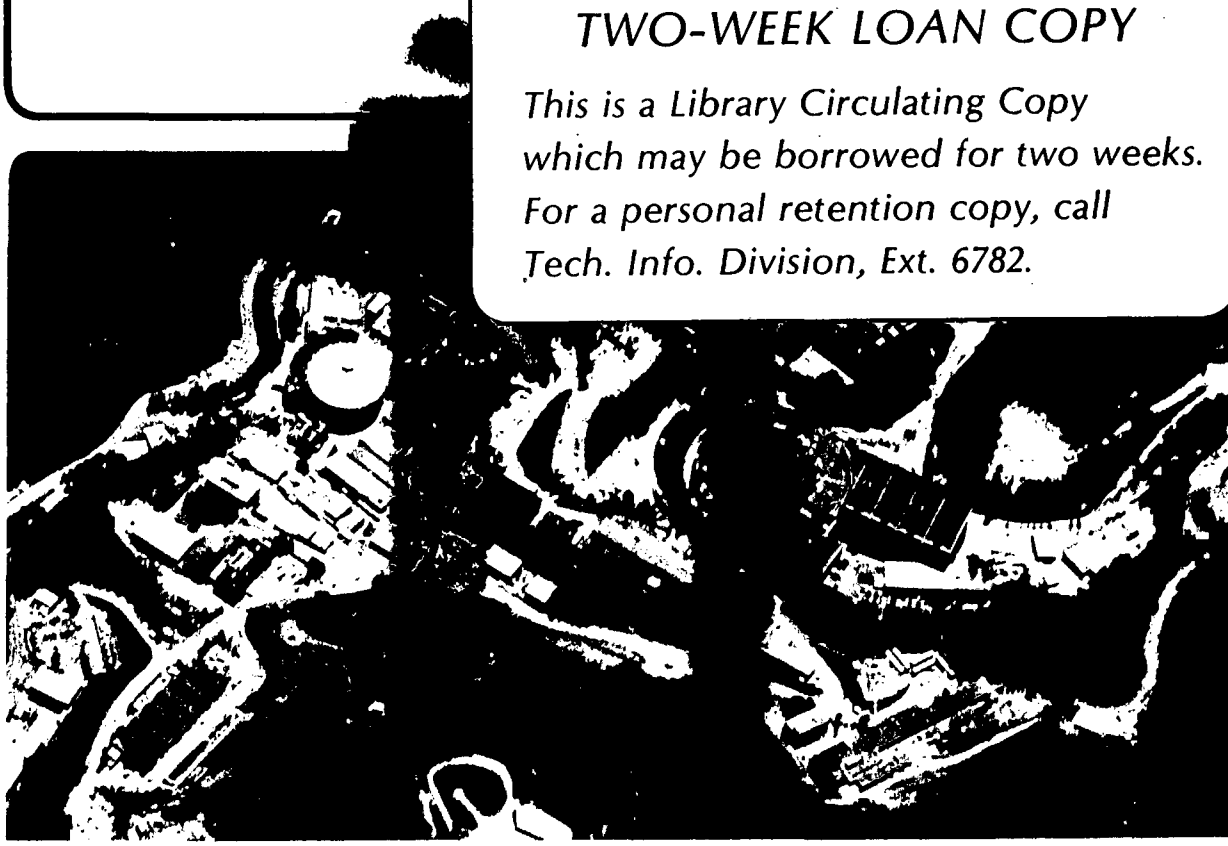

Prepared for the U.S. Department of Energy under Contract DE-AC03-76SF00098

LBL-15590 c.2

DISCLAIMER

This document was prepared as an account of work sponsored by the United States Government. While this document is believed to contain correct information, neither the United States Government nor any agency thereof, nor the Regents of the University of California, nor any of their employees, makes any warranty, express or implied, or assumes any legal responsibility for the accuracy, completeness, or usefulness of any information, apparatus, product, or process disclosed, or represents that its use would not infringe privately owned rights. Reference herein to any specific commercial product, process, or service by its trade name, trademark, manufacturer, or otherwise, does not necessarily constitute or imply its endorsement, recommendation, or favoring by the United States Government or any agency thereof, or the Regents of the University of California. The views and opinions of authors expressed herein do not necessarily state or reflect those of the United States Government or any agency thereof or the Regents of the University of California.

LONGITUDINAL STABILITY OF A COASTING BEAM IN A RESISTIVE VACUUM CHAMBER WITH CYLINDRICAL RESONANT CAVITY

PART II

GRAPHS AND A FORMULA FOR THE COUPLING IMPEDANCE*

Robert L. Warnock

Lawrence Berkeley Laboratory
University of California
Berkeley, California 94720 USA

and

George R. Bart

Truman College
Chicago, Illinois 60640 USA

* This work was supported by the Director, Office of Energy Research, Office of High Energy and Nuclear Physics, Division of High Energy Physics of the U.S. Department of Energy under Contract DE-AC03-76SF00098.

ABSTRACT

The longitudinal coupling impedance of a cylindrical tube with pillbox cavity is computed by means of cavity mode equations derived in Part I. The equations are solved by a method in which the resonant mode is first eliminated. The method leads to a rapidly convergent iteration which takes account of cavity-tube coupling in a stepwise manner. A similar procedure should be effective in other electromagnetic problems with resonances. Numerical results are given for a wide range of parameters, with full account of wall resistance. The resistance of the cavity end walls is more effective in reducing the Q than was previously supposed. The formula for the impedance in the limit of small tube radius, modified by a simple factor, approximates the numerical values and provides an overview of parameter dependences. For possible applications to heavy ion beams we give results for non-relativistic velocities, and study the exponential decrease of impedance with cavity depth which occurs at low velocity.

1. INTRODUCTION

In part I we began a study of longitudinal stability of a coasting beam in a model vacuum chamber consisting of a round tube with a cavity formed by double-step discontinuities of radius.[1] Extending earlier work of Keil and Zotter,[2] we found equations for the Fourier coefficients of the electric field inside the cavity. A solution of those equations leads directly to the coupling impedance, which in turn yields stability criteria and rise-times of instabilities through the dispersion relation. We transformed the kernel matrix of the equations so as to make it easier to compute and to make explicit its behavior in the limit of small tube radius. Also, we used a non-harmonic Fourier series in the cavity region, in order to include resistivity on the cavity end walls as well as on cylindrical surfaces.

In the present paper we apply the equations to obtain numerical results and an analytical formula for the impedance. The analytical result is accurate for small b/d (b = tube radius, d = cavity radius), but with a simple modification it also leads to good estimates for larger b/d and provides general guidance about parameter dependences.

For an accurate numerical solution at a cavity resonance we make a further transformation, in which the resonant cavity mode amplitude is eliminated in favor of all the non-resonant ones. Being devoid of large resonant amplitudes, the new equations are easily solved by iteration; in fact, the lowest iterate provides a good approximate solution.

To deal with the infinite set of unknowns that the equations entail we employ a mapping and interpolation technique to approximate the effect of all high coupled modes in terms of just a few of them.

Thus we take advantage of the smooth dependence of high modes on mode number, and avoid the customary truncation in which only the first few modes are retained. We find that in fact the high modes do not have much effect. We compare the impedance computed with the ten lowest modes to that computed with all modes and find a difference of only 1% (at maxima of the impedance). Initially it was not obvious that high modes would be unimportant, since the asymptotic decrease of amplitudes with mode number is not very rapid.

In Section 2 we derive the expression for the impedance in the limit of small tube radius from the general equations of Part I. The formula obtained, Eq. (2.24), includes an important effect of non-zero tube radius; namely the exponential cut-off of impedance at small beam velocity.

In Section 3 we show how to eliminate the resonant mode amplitude from the general equations. The resulting iterative method for calculating the impedance is summarized in Eqs. (3.12)-(3.15).

In Section 4 we review our numerical procedures, including the interpolation method for high coupled modes. The latter may be of some general interest.

In Section 5 we describe scaling laws and other features which simplify the problem of specifying the parameter dependence of the impedance.

Section 6 contains graphs of numerical results and a formula, (6.11), which roughly summarizes the results in a quasi-analytic form.

A reader not interested in derivations may directly consult Sections 5 and 6 for values of the impedance.

We have changed the organization of the paper since Part I was written. We now plan a Part III, to include calculations of the rise times of instabilities, stability limits, and the Fredholm theory of the infinite-dimensional mode equations. It will also include some graphs of the smooth resistive tube impedance, which are relevant in the case of non-relativistic beams.

References to equations in Part I will have I as a prefix; for instance (I-4.23).

2. LIMITING CASE OF SMALL TUBE RADIUS

We treat the limit $b \to 0$ with a/b held constant, where b is the tube radius and a the beam radius. Actually, we pass to the limit only in certain elements of the general formula for the coupling impedance, and thereby obtain a simple expression which is valid for small but non-zero tube radius. The full formula for the impedance as calculated from the cavity mode equations is given in (I-4.23) and (I-4.24). It consists of the impedance Z_t of a smooth tube with resistive wall, plus the main term Z_c due to the cavity. Of course, Z_c contains all effects of coupling between tube and cavity, and becomes a pure cavity impedance only in the limit of small b. For present purposes Z_c may be written for tube mode n in the form

$$Z_c = \frac{-iZ_o}{\pi f} \frac{2gd}{b^2} \frac{I_1(\chi_n a)}{\chi_n a I_o^2(\chi_n b)} \left(N(1-RE)^{-1} R\tilde{N} \right)_{nn} . \qquad (2.1)$$

Here $Z_o = (\mu_o/\varepsilon_o)^{1/2} = 120\pi\,\Omega$ is the impedance of free space, 2g and d are length and radius of the cavity, respectively, and f is the dimensionless frequency

$$f = \frac{\omega d}{c} . \qquad (2.2)$$

We have dropped terms proportional to the dimensionless tube resistivity η_t, which vanish at small b. We have used the plasma resonance condition ($\omega/k_n \cong \beta c$) to replace k_n in (I-4.23) by f in the first factor of (2.1).

The arguments of the modified Bessel functions I_o, I_1 are given in terms of the radial wave number χ_n of the tube region, namely

$$\chi_n^2 = k_n^2 - (\omega/c)^2 \quad , \qquad k_n = n/R \quad . \tag{2.3}$$

The fields have longitudinal period $2\pi R$, so that R may be interpreted as the ring radius. The quantity in brackets in (2.1) is a matrix made up of the infinite dimensional matrices N, $\tilde{N}$, E, and R; the subscript nn denotes the n-th diagonal element. The matrix N (related to $\tilde{N}$ by $\tilde{N}_{sn} = N_{-ns} = (-1)^s N_{ns}$) is defined in (I-3.53,I-3.55); the element N_{ns} represents the degree of overlap between axial mode s of the cavity and axial mode n of the tube at the tube-cavity interface. The diagonal matrix $R = \{R_s \delta_{st}\}$, associated with radial variation of the fields in the cavity region, is defined in (I-3.60,I-3.30). The matrix E is the kernel of the equations for cavity mode amplitudes. It was derived initially in the form (I-3.69), and was then transformed by the Watson-Sommerfeld method to give expression (I-5.18). The transformation has several advantages, one being that it puts E in the form $E = \Delta + F$, where Δ is diagonal and F vanishes in the limit $b \to 0$. Indeed, a simple bound on the summand of the sum (I-5.18) defining F shows that $F = \mathcal{O}(b)$, $b \to 0$. In the small-b limit the last factor in (2.1) is then simply

$$\sum_s (-1)^s N_{ns}^2 \frac{R_s}{1-R_s\Delta_s} \quad . \tag{2.4}$$

The condition for a resonance in cavity mode s = r at frequency $\omega = \omega_r$ is that the r-th term of this sum have a pole, or

$$1 - \Delta_r(\omega_r)R_r(\omega_r) = 0 \quad . \tag{2.5}$$

The frequency ω_r has a small negative imaginary part, which vanishes in the limit of zero cavity wall resistivity. Stability limits or rise times of instabilities are determined by solutions ω of the dispersion relation with $\mathrm{Im}\omega$ zero or slightly positive. As will be clear later when we compute rise times, ω is so close to one of the resonance poles and so far from the others that only the term in (2.4) with the close pole need be retained. Moreover, the term retained (say the r-th term) may be adequately represented as purely a pole in the ω plane at ω_r. Thus, the resonant impedance takes the form

$$Z_c = \frac{-2iZ_o gd}{\pi b^2} \left(\frac{I_1(\chi_n a)(-)^r N_{nr}^2 R_r}{f\chi_n a I_o^2(\chi_n b)} \right)_{\omega=\omega_r} \frac{1}{\mathcal{D}'(\omega_r)(\omega-\omega_r)} \tag{2.6}$$

where

$$\mathcal{D}(\omega) = 1 - \Delta_r(\omega)R_r(\omega) \quad . \tag{2.7}$$

The imaginary part of ω_r is significant only in the small demoninator factor $\omega - \omega_r$; elsewhere we may put $\omega_r = \mathrm{Re}\omega_r$.

To put (2.6) in a tractable form for small b we first recall the definitions of Δ_r and R_r in (I-5.19) and (I-3.60) to obtain

$$\mathcal{D} = 1 - \frac{I_1(\Gamma_r b)}{I_o(\Gamma_r b)-(\eta_c/\Gamma_r b)I_1(\Gamma_r b)} \; \frac{R_o(\Gamma_r b,\Gamma_r d)-(\eta_c/\Gamma_r b)S_o(\Gamma_r b,\Gamma_r d)}{R_1(\Gamma_r b,\Gamma_r d)-(\eta_c/\Gamma_r b)S_1(\Gamma_r b,\Gamma_r d)} \quad . \tag{2.8}$$

The R_i and S_i are "cross products" of Bessel functions defined in (I-3.17, 3.18), and Γ_r is the radial wave number in the cavity region,

$$\Gamma_r^2 = -(\omega/c)^2 + \alpha_r^2 = -(\omega/c)^2 + (r\pi/2g)^2 - (2-\delta_{ro})\kappa(\omega)/g^2 + \mathcal{O}(\kappa^2) \quad . \tag{2.9}$$

The small dimensionless parameters η_t, η_c refer to cylindrical tube and cavity surfaces, respectively, while κ is a similar parameter for the planar cavity end walls. The definitions are

$$\eta_{t,c} = -\varepsilon_o(\mu/\sigma)_{t,c}^{1/2}\, b\, p^{3/2} \quad , \quad \kappa = -\varepsilon_o(\mu/\sigma)_e^{1/2}\, g\, p^{3/2} \tag{2.10}$$

where μ and σ are magnetic permeability and electrical conductivity of the appropriate walls labeled t, c, e. The Laplace transform variable p is equal to $-i\omega$, and the function $p^{1/2}$ is defined so that its real part is positive in the right-half p-plane, as follows from the demand that fields decrease exponentially within the conductors (Appendix B, Part I). Thus for ω in the upper half-plane, $0 < \arg\omega < \pi$, we have $\mathrm{Re}\, p^{1/2} > 0$ and the representation

$$p^{1/2} = (-i\omega)^{1/2} = \frac{1-i}{2^{1/2}}|\omega^{1/2}|\exp(\frac{i}{2}\arg\omega) \quad . \tag{2.11}$$

Near a resonance frequency the expression (2.8) may be represented at small b as

$$\begin{aligned} \mathcal{D} \simeq\ & [2dI_1(\Gamma_r d)/\Gamma_r b^2]\cdot[1 + \mathcal{O}(b)] \\ & \cdot[I_o(\Gamma_r d) - (\eta_c/\Gamma_r b)I_1(\Gamma_r d) + \mathcal{O}(b^3)] \quad . \end{aligned} \tag{2.12}$$

This result is derived by combining the two terms of (2.8) with the help of (I-3.21); the denominator of the resulting expression is then evaluated at the point where the numerator vanishes to yield the approximation (2.12). To determine ω_r we drop the terms that vanish with b and find the zero of

$$f(\omega) = I_o(\Gamma_r d) - (\eta_c/\Gamma_r b)I_1(\Gamma_r d) \tag{2.13}$$

by Newton's method. Since η_c is small compared to 1, a good point to start a Newton iteration is $\omega = \hat{\omega}$, where $I_o(\Gamma_r(\hat{\omega})d) = 0$. Then to sufficient accuracy,

$$\omega_r = \hat{\omega} - f(\hat{\omega})/f'(\hat{\omega}) \quad . \tag{2.14}$$

We determine $\hat{\omega}$ in turn by a separate application of Newton's method, beginning at ω_o, which is the value $\hat{\omega}$ would have if the end walls were perfectly conducting; namely,

$$\omega_o = \pm(c/d)[\, j_{oi}^2 + (r\pi d/2g)^2\,]^{1/2} \quad . \tag{2.15}$$

Here j_{oi} is the i-th zero of the Bessel function J_o. A short calculation yields

$$\omega_r = \hat{\omega} - \eta_c(\hat{\omega})c^2/bd\hat{\omega} + \mathcal{O}(\eta_c^2, \eta_c\kappa) \tag{2.16}$$

and

$$\hat{\omega} = \omega_o - \kappa(\omega_o)c^2/(1+\delta_{ro})g^2\omega_o + \mathcal{O}(\kappa^2) \quad , \tag{2.17}$$

hence

$$\omega_r = \omega_o - (c^2/\omega_o)\ [\ \eta_c(\omega_o)/bd + \kappa(\omega_o)/(1+\delta_{ro})g^2\ ] \quad . \tag{2.18}$$

By (2.10) and (2.11) this result may be written as

$$\omega_r = \omega_o - (\pm 1+i)\varepsilon_o c^2|\omega_o^{1/2}|[\ (\mu/2\sigma)_c^{1/2}/d + (\mu/2\sigma)_e^{1/2}/(1+\delta_{ro})g\ ] \quad . \tag{2.19}$$

Here and in the following we neglect terms of second and higher order in resistivity, which are indeed negligible in the frequency range of interest. In (2.19) the choice of sign in the second term is to agree with the choice in the definition (2.15) of ω_o. The two signs of ω_o give the same value of $\mathrm{Im}\,\omega_r$ and opposite values of $\mathrm{Re}\,\omega_r$, and hence lead to the same rise time. We may then restrict attention to the positive values of ω_o, each of which is indexed by a radial mode number i of the Bessel function zero and an axial mode number r. The difference between $\mathrm{Re}\omega_r$ and ω_o, being $\mathcal{O}(\eta_c,\kappa)$, is not significant in the following; we put $\mathrm{Re}\omega_r = \omega_o$. If we take $\mu_c = \mu_e = \mu_o$, then (2.19) yields

$$\mathrm{Im}\,\omega_r = -(c/d)\ [j_{oi}^2 + (r\pi d/2g)^2]^{1/4}[2Z_o\sigma_c d]^{-1/2}[1 + d(\sigma_c/\sigma_e)^{1/2}/(1+\delta_{ro})g] \quad . \tag{2.20}$$

It remains to determine the constants $R_r(\omega_r)$ and $\mathcal{D}'(\omega_r)$ of (2.6). Evaluating the derivative of $f(\omega)$ for small b, we find

$$\mathcal{D}'(\omega_r) = -2\omega_o\left[\frac{d^2J_1(j_{oi})}{bcj_{oi}}\right]^2 + \mathcal{O}(\eta_c, \kappa) \quad , \tag{2.21}$$

where J_1 is the ordinary Bessel function. In view of (2.5), we may calculate R_r as $1/\Delta_r$ which at small b has the value

$$1/\Delta_r = 4 - 2\delta_{ro} \quad , \qquad b \to 0. \tag{2.22}$$

This result follows from (I-5.19), (I-3.57), (I-3.41), and (I-3.42). From (I-3.55) and (I-3.63) it is seen that

$$(-)^r N_{nr}^2 = |N_{nr}(\kappa=0)|^2 + \mathcal{O}(\kappa) \quad . \tag{2.23}$$

With the help of (2.20)-(2.23) we evaluate (2.6) on the real ω-axis at the peak of the resonance to obtain

$$Z_c(\omega=\mathrm{Re}\omega_r) = \frac{4Z_o g}{\pi d}\ \frac{(2\sigma_c Z_o d)^{1/2}}{(\omega_o d/c)^{5/2}}\left(\frac{j_{oi}}{J_1(j_{oi})}\right)^2$$
$$\times \frac{1}{1 + \delta_{ro} + (d/g)(\sigma_c/\sigma_e)^{1/2}}\ \frac{I_1(\chi_n a)}{\chi_n a I_o^2(\chi_n b)}\ |N_{nr}(\kappa=0)|^2 \quad . \tag{2.24}$$

Here χ_n is to be evaluated by (2.3) with $\omega = \omega_o$, and ω_o is given in terms of the mode numbers (i, r) by (2.15). In (2.24) we have dropped a complex factor $1 + \mathcal{O}(\eta_c, \kappa)$, which differs from unity only by terms which are typically of order 10^{-4}.

The Bessel function factor of (2.24) has a small-b limit of 1/2:

$$\frac{I_1(\chi_n a)}{\chi_n a I_o^2(\chi_n b)} \rightarrow 1/2 \ , \qquad b \rightarrow 0 \ . \tag{2.25}$$

We purposely avoid taking this limit, however, because at non-relativistic velocities and small but non-zero b, the factor may differ greatly from 1/2. When formula (2.24) for the impedance is left as it stands, it agrees approximately with the exact results of Section 6, for small non-zero b.

The factor $|N_{nr}|$ of (2.24) is similar to the transit time factor as usually defined for active r.f. cavities. It is proportional to the energy change of a particle, due to the beams's own field, as the particle traverses the cavity. We have

$$|N_{nr}(\kappa=0)|^2 = \left(\frac{k_n g}{(k_n g)^2-(r\pi/2)^2}\right)^2 \times \begin{pmatrix} \sin^2 k_n g \ , & r \text{ even} \\ \cos^2 k_n g \ , & r \text{ odd} \end{pmatrix} \ . \tag{2.26}$$

The formula (2.24) provides insight as to how the impedance depends on parameters, even at large b/d; see Sections 5 and 6.

From (2.20) and $\mathrm{Re}\,\omega_r \simeq \omega_o$ we obtain the quality factor in the familiar form

$$Q = \frac{\mathrm{Re}\,\omega_r}{|2\mathrm{Im}\,\omega_r|} = \frac{d/\delta}{1 + \frac{1}{1+\delta_{ro}} \frac{d}{g} \left(\frac{\sigma_c}{\sigma_e}\right)^{1/2}} \tag{2.27}$$

where the skin depth δ is defined by

$$\delta = (\mu_o \sigma \omega_o/2)^{-1/2} \ . \tag{2.28}$$

3. ELIMINATION OF RESONANT MODE AMPLITUDES

In Part I we gave two different formulas for the impedance, one based on solving equations for the cavity mode amplitudes and the other on equations for the tube mode amplitudes. Although both formulas are exact, the former is best suited to the case of deep cavities, and the latter to shallow cavities. In the present paper we use the cavity mode formula, but actually apply it to shallow as well as deep cavities: we work in the interval $.2 < b/d < .9$. From a physical viewpoint it seems questionable to use this formula for b/d as large as 0.9, but we experience no difficulties of convergence in doing so.

As is seen from (I-4.24) or (2.1), the main problem in finding the impedance of arbitrary b is to compute $[(1-RE)^{-1}R\tilde{N}]_{sn}$; i.e., to solve the following system of equations for the vector X:

$$(1-RE)X = (R\tilde{N})_{.n} \quad . \tag{3.1}$$

We use the notation $(R\tilde{N})_{.n}$ for the vector with components $R_s\tilde{N}_{sn}$, $s = 1, 2, \ldots$. A cavity resonance is associated with a pole of the impedance just below the real ω-axis, which arises from a zero of the determinant,

$$\det(1-RE) = 0 \quad . \tag{3.2}$$

Since we must evaluate the impedance near the pole in treating beam stability, our problem is to solve the system (3.1) when it is nearly singular. From a numerical point of view it is not advisable to attack directly an ill-conditioned (almost singular) system. Accordingly we seek to replace (3.1) by an equivalent well-conditioned system.

The components of X are labeled by $s = 1, 2. \ldots$, the axial field mode number in the cavity region. In fact, X_s is proportional to the cavity electric field amplitude in mode s, due to a charge perturbation in tube axial mode n. Numerical calculations show that a resonance is largely confined to a single mode $s = r$ even at large b/d; i.e., X_r becomes much larger than all the other X_s for ω near a zero of the determinant. That suggests that the singularity could be avoided by eliminating the large amplitude X_r from the equations to be solved.

The matrix E has the form

$$E = (F+\Delta)(1-\eta_t vR^{-1}) \quad , \tag{3.3}$$

where F is given by an infinite series, the first term of (I-5.18), and the diagonal matrices Δ, v, and R are defined in (I-5.19), (I-3.65), and (I-3.60). The term $\eta_t vR^{-1}$, which we could neglect in comparison to 1 at small b/d, is in general not very important, but we retain it anyway. We substitute (3.3) in (3.1) and rearrange to obtain

$$(1-Q\tilde{F})X = (Q\tilde{N})_{.n} \tag{3.4}$$

where

$$\tilde{F} = F(1-\eta_t v R^{-1}) \quad , \tag{3.5}$$

$$Q = R[1-\Delta(R-\eta_t v)]^{-1} \quad . \tag{3.6}$$

Since the components of F are small compared to the diagonal components of Δ, we have separated F and Δ in (3.4), to prepare for a later expansion in powers of F.

We take the resonant mode number to be s = r, and solve (3.4) for the non-resonant amplitudes in terms of the resonant one, X_r:

$$X_s = \sum_{t\neq r} \left\{1 - Q\tilde{F}\right\}^{-1}_{st} Q_t \left(\tilde{F}_{tr} X_r + \tilde{N}_{tn} \right) \quad , \quad s \neq r \quad . \tag{3.7}$$

Here the curly brackets mean that the matrix within the brackets is restricted to the non-resonant subspace. If we now substitute (3.7) in (3.4), and take the r-th component of (3.4), we obtain a linear equation for X_r alone. That equation has the solution

$$X_r = Q_r \frac{\tilde{N}_{rn} + \sum_{t,u\neq r} \tilde{F}_{rt} \left\{1-Q\tilde{F}\right\}^{-1}_{tu} Q_u \tilde{N}_{un}}{1-Q_r \left(\tilde{F}_{rr} + \sum_{t,u\neq r} \tilde{F}_{rt} \left\{1-Q\tilde{F}\right\}^{-1}_{tu} Q_u \tilde{F}_{ur} \right)} \quad . \tag{3.8}$$

The non-resonant components of X are now constructed by putting this result for X_r into the right-hand side of (3.7).

By expanding the resolvent matrix $\{1 - Q\tilde{F}\}^{-1}$ in powers of $\tilde{F}$, we obtain the desired perturbative method:

$$\left\{1 - Q\tilde{F}\right\}^{-1}_{st} = 1 + Q_s \tilde{F}_{st} + \sum_{u\neq r} Q_s \tilde{F}_{su} Q_u \tilde{F}_{ut}$$

$$+ \sum_{u,v\neq r} Q_s \tilde{F}_{su} Q_u \tilde{F}_{uv} Q_v \tilde{F}_{vt} + \ldots\ldots, \qquad s \neq r \quad . \tag{3.9}$$

Thus by (3.8) and (3.9) we express X_r as the ratio of two series, each in ascending powers of the matrix $\{Q\tilde{F}\}$. A resonance pole of X_r in the ω plane comes from a zero of the series forming the denominator $\mathcal{D}$, namely

$$\mathcal{D}(\omega) = 1 - Q_r \tilde{F}_{rr} - \sum_{t\neq r} Q_r \tilde{F}_{rt} Q_t \tilde{F}_{tr}$$

$$- \sum_{t,u\neq r} Q_r \tilde{F}_{rt} Q_t \tilde{F}_{tu} Q_u \tilde{F}_{ur} + \ldots\ldots \tag{3.10}$$

The same pole occurs in X_s, $s \neq r$, but in general with a smaller residue due to an extra factor of $\tilde{F}$. Notice that we could not have obtained a pole by attempting a simple iterative solution of the original equation (3.4). Our procedure is analogous to the method of Jost in quantum mechanical scattering theory.[3] In the latter the numerator and denominator in the so-called N/D representation of the scattering amplitude, rather than the amplitude itself, are expanded in perturbation series. Resonances or bound states correspond to zeros of D in the energy plane, and are not accessible by the Born perturbation series for the amplitude itself.

Using the solution (3.8), (3.7) of equation (3.1). we can evaluate the formula for the impedance (I-4.23, 4.24) as follows:

$$Z = Z_t + Z_c \quad , \tag{3.11}$$

where Z_t is the impedance of the smooth tube and

$$Z_c = \frac{-2iZ_o gd}{\pi f b^2} \frac{I_1(\chi_n a)}{\chi_n a I_o^2(\chi_n b)(1-\eta_t I_n)^2} \tag{3.12}$$

$$\times \sum_{s=0}^{\infty} N_{ns}(1-\eta_t v_s R_s^{-1})(A_s+B_s X_r)$$

where

$$A_r = 0 \ , \qquad B_r = 1 \ , \tag{3.13}$$

$$A_s = \sum_{t\neq r} \left\{ 1-Q\tilde{F} \right\}^{-1}_{st} Q_t \tilde{N}_{tn} \ , \qquad s \neq r \ , \tag{3.14}$$

$$B_s = \sum_{t\neq r} \left\{ 1-Q\tilde{F} \right\}^{-1}_{st} Q_t \tilde{F}_{tr} \ , \qquad s \neq r \ . \tag{3.15}$$

$$I_n = I_1(\chi_n b)/\chi_n b I_o(\chi_n b) \ . \tag{3.16}$$

The resonant amplitude X_r is given in terms of the same A_s and B_s:

$$X_r = Q_r \frac{\tilde{N}_{rn} + \sum_{s\neq r} \tilde{F}_{rs} A_s}{1-Q_r(\tilde{F}_{rr} + \sum_{s\neq r} \tilde{F}_{rs} B_s)} \ . \tag{3.17}$$

We have reduced the calculation of the impedance to the solution of two linear systems, both with the same well-conditioned matrix of coefficients:

$$\left\{ 1 - Q\tilde{F} \right\} A = Q\tilde{N}_{.n} \ , \tag{3.18}$$

$$\left\{ 1 - Q\tilde{F} \right\} B = Q\tilde{F}_{.r} \ . \tag{3.19}$$

Of course, these equations could be solved by a non-iterative method (say Gaussian elimination), but we have found that the iteration (3.9) is an efficient way to proceed. In fact we find that a good approximation to Z_c is obtained, even at large b/d, if just the zeroth order values of A and B are used; namely, $A_s = Q_s \tilde{N}_{sn}$, $B_s = Q_s \tilde{F}_{sr}$, $s \neq r$. In that approximation only the r-th row of the matrix $\tilde{F}$ is needed to calculate the impedance, and the required computer time is very small.

In Section 6 we give numerical results from evaluation of (3.12). Near the resonance energy, Z_c may be represented accurately as a pole plus a small constant background:

$$Z_c = \frac{ic_1}{\omega-\omega_r} + c_2 \ . \tag{3.20}$$

Since stability limits or growth times of instabilities are determined by a region of the ω-plane very close to ω_r, we can neglect the background c_2. The imaginary part of c_1 is negligible compared to its real part, so that Z_c in the relevant region is determined by three real numbers: c_1, $\mathrm{Re}\,\omega_r$, $\mathrm{Im}\,\omega_r$. We tabulate the equivalent three numbers

$$Z_c(\omega=\mathrm{Re}\,\omega_r) = \frac{c_1}{|\mathrm{Im}\,\omega_r|} \ , \qquad Q = \frac{\mathrm{Re}\,\omega_r}{2|\mathrm{Im}\,\omega_r|} \ , \qquad f = (\mathrm{Re}\,\omega_r)d/c \ . \tag{3.21}$$

Notice that only the term in (3.12) proportional to X_r involves the pole; the rest may be dropped.

The relevant tube mode number n for the stability question is given by the plasma resonance condition $\omega/k_n \approx \beta c$. For evaluation of (3.12) we take the non-integer value

$$n = (\mathrm{Re}\,\omega_r)R/\beta c \quad . \tag{3.22}$$

Thus, in our graphs of $Z_c(\omega = \mathrm{Re}\omega_r)$ versus geometrical parameters the value of n varies continuously along a curve, since ω_r changes with geometrical parameters. Had we properly taken the integer closest to (3.22) for n, there would be step discontinuities in the curves where n changes by one unit. The value of n is typically so large that the discontinuities are of negligible magnitude.

For non-relativistic high current beams there is a special situation (occurring in a narrow range of parameters) in which two neighboring tube modes participate. A 2 x 2 submatrix of an infinite-dimensional impedance matrix is then involved. This case will be discussed in Part III; as far as calculation of the impedance is concerned it presents no new problems.

4. NUMERICAL METHODS

We review those aspects of our computer program which have been crucial in minimizing computer time and ensuring accuracy.

(1) Coefficients of the Mode Amplitude Equations.

A large fraction of the computation time is used in calculating the matrix F of (3.5), which is given by the cubically convergent infinite series, (I-5.18). The series can be computed to adequate accuracy by retaining 1000 terms, but that becomes rather expensive when we evaluate F at many different frequences while locating the pole of the impedance in the frequency plane. Fortunately, only the first few terms of the series depend appreciably on frequency, so that the remainder need be recomputed only when a large change of parameters is made. Better yet, the tail of the series is well approximated by a simple integral, which can be evaluated as a logarithm. This approximation is uniformly valid over the parameter range of interest, and allows us to write F as N terms of the series (I-5.18) plus the remainder,

$$F^R_{st} = -(g/2\pi b) \times \begin{cases} \dfrac{1}{x_s^2 - x_t^2}\, \ln\left(\dfrac{\lambda^2 + x_s^2}{\lambda^2 + x_t^2}\right) , & s \neq t , \\[2ex] \dfrac{1}{\lambda^2 + x_s^2} , & s = t . \end{cases}$$

$$\lambda = (N + 1/2)\pi g/b \tag{4.1}$$

Here $x_s = \alpha_s g = s\pi/2 + O(\kappa)$; see (2.6) or (I-3.41, I-3.42). A rather small value of N can be used. The graphs of Section 6 were computed with N = 25, and are virtually indistinguishable from graphs

obtained with N = 1000.

(2) Finding the Pole of the Impedance.

To locate a pole of the impedance (equivalently, to find a cavity resonance frequency and Q factor) we have to solve the non-linear equation

$$\mathcal{D}(f) = 0 \quad , \tag{4.2}$$

where $f = \omega d/c$ and $\mathcal{D}$ is the denominator function (3.10). We do so by the method of regula falsi,[4] which is Newton's method modified so that the derivative is approximated as a difference quotient. Thus, the iteration to find a root is given by

$$f_{n+1} = f_n - \mathcal{D}(f_n) \frac{f_n - f_{n-1}}{\mathcal{D}(f_n) - \mathcal{D}(f_{n-1})} \quad . \tag{4.3}$$

For $b/d \lesssim .5$ and $g/d \gtrsim 1$, the iteration converges quickly if the zeroth approximation f_o is taken to be the value of f for b = 0 as given in (2.15). (Once f_o is chosen, f_1 is taken to be $f_o + \Delta f$ with Δf any number of order $10^{-3} - 10^{-4}$.) Starting in the region of small b/d and large g/d, we vary b/d and g/d in small steps to cover the entire parameter range. We begin each iteration with a linear extrapolation from a previous solution of (4.2). If x is the parameter to be incremented, then differentiation of $\mathcal{D}(f, x) = 0$ gives

$$\frac{\partial f}{\partial x} = - \frac{\partial \mathcal{D}/\partial x}{\partial \mathcal{D}/\partial f} \tag{4.4}$$

and the desired extrapolation is

$$f(x+\Delta x) = f(x) - \frac{\partial \mathcal{D}/\partial x}{\partial \mathcal{D}/\partial f} \Delta x \quad . \tag{4.5}$$

For the derivatives in (4.5) we use an approximation to $\partial\mathcal{D}/\partial f$ already obtained in the iteration for parameter x, and

$$\frac{\partial \mathcal{D}}{\partial x} \simeq \frac{\mathcal{D}(f(x), x+\Delta x) - \mathcal{D}(f(x), x)}{\Delta x} \quad . \tag{4.6}$$

Since $\mathcal{D}$ is the difference of two terms each of order 1, the best solution of (4.2) with the 32 bit arithmetic used corresponds to $|\mathcal{D}| \sim 10^{-6} - 10^{-7}$. We usually obtain a solution of that accuracy in 3 or 4 steps of iteration (4.3). The value of the derivative $\mathcal{D}'$, obtained as a difference quotient at the last step of the iteration, is not reliable due to round-off error: $\mathcal{D}(f_n)$ and $\mathcal{D}(f_{n-1})$ are too close together. Since we need a good value of $\mathcal{D}'$ to compute the impedance at the resonance maximum (to find the residue of the resonance pole), we finally recompute the derivative at the solution f obtained, by using larger increments of f in a 4-point formula from cubic splines.[5] The accuracy of f and $\mathcal{D}'(f)$ was checked by doing some double-precision runs, and was found to be more than adequate.

(3) Treatment of High Coupled Modes

The equations of Section 3 involve infinite sums over axial cavity mode munber s,

$$\sum_{s=0}^{\infty} \phi_s \quad , \tag{4.7}$$

where ϕ_s is any one of several functions appearing in (3.7)-(3.19). All of those functions have in common that they decrease more rapidly than $s^{-3+\varepsilon}$, $s \to \infty$, for any $\varepsilon > 0$. This assertion may be verified directly for those cases in which ϕ_s is known explicitly (as in any term of (3.9)). When ϕ_s involves the unknown A_s or B_s, the assertion follows from the Fredholm theory of equations (3.18), (3.19), to be developed in Part III. The ϕ_s are smooth (in fact analytic) functions of s, although they are evaluated only at integer s in (4.7). We take advantage of the smooth s-dependence to approximate the tail of (4.7) in terms of ϕ_s at just a few large non-integer values of s.

A smooth function f(x) on a finite interval [0, m], where m is a positive integer, may be approximated in terms of cardinal spline functions $\beta_p(x)$ as follows:[5]

$$f(x) \simeq \sum_{p=0}^{m} f(p)\beta_p(x) \quad . \tag{4.8}$$

In (4.7) we leave the first few terms of the sum as they stand, and map the remaining infinite interval of s, say $s > s_o$, onto the finite interval [0 , m] by some mapping s(x) with inverse x(s). For $s > s_o$ we first multiply ϕ_s by $(s + a)^{3-\varepsilon}$, ε small and $a > 0$, to remove most of the asymptotic variation with s. We then represent the product by splines,

$$\phi_{s(x)}(s(x)+a)^{3-\varepsilon} \simeq \sum_{p=0}^{m} \phi_{s(p)}(s(p)+a)^{3-\varepsilon}\beta_p(x) \quad . \tag{4.9}$$

Finally we put (4.9) into (4.7) and reverse the order of s and p sums to obtain

$$\sum_{s=0}^{\infty} \phi_s \simeq \sum_{s=0}^{s_o-1} \phi_s + \sum_{p=0}^{m} \phi_{s(p)} w_p \quad , \tag{4.10}$$

$$w_p = (s(p)+a)^{3-\varepsilon} \sum_{s=s_o}^{\infty} \beta_p(x(s))(s+a)^{-3+\varepsilon} \quad . \tag{4.11}$$

The ϕ_s depend on various parameters, but the weights w_p are independent of ϕ_s and may be computed and stored once for all.

The accuracy of (4.10) will depend strongly on the choice of the mapping s(x). For guidance in making a rational choice, imagine that we had to evaluate the trivial integral,

$$\int_1^\infty \frac{ds}{s^3} \quad , \tag{4.12}$$

by numerical quadrature. Any quadrature rule would give the right answer if we first made the change of variable $x = 1/s^2$, which renders the integrand constant and maps the infinite interval onto a finite one. In particular, a rule based on equally spaced mesh points in the variable x would be good. Since our sums are roughly cubically convergent, a corresponding inverse square mapping seems appropriate for our spline approximation. We take

$$\frac{x}{m} = 1 - \left(\frac{s_o+a}{s+a}\right)^2 \quad . \tag{4.13}$$

Actually, we use a refinement of the above formula (4.10), to make the function approximated by splines as nearly constant as possible. The functions ϕ_s have another matrix index t which we have suppressed heretofore; in fact, the sums to be evaluated have the form

$$\sum_{s=0}^{\infty} F_{ts}\psi_s \quad , \tag{4.14}$$

where F is the matrix of coefficients discussed in Section 3, and ψ_s decreases faster than $s^{-1+\varepsilon}$ for any $\varepsilon > 0$. The behavior of F_{ts} at large but not asymptotic s depends considerably on t. The dependence on s and t is similar to that of the function F^R_{st} of (4.1), which suggests that it would be useful to divide the summand of (4.14) by F^R_{st} before making the spline approximation. Accordingly we define

$$\omega(s,t) = \frac{(s+a)^{1-\varepsilon}}{F^R_{st}(N=0, x_s = s\pi/2)} \tag{4.15}$$

and make a spline approximation to $F_{ts}\ \psi_s\omega(s,t)$, in the manner of (4.10). We then get t-dependent weights instead of (4.11),

$$w_p(t) = \omega(s(p),t) \sum_{s=s_o}^{\infty} \frac{\beta_p(x(s))}{\omega(s,t)} \quad , \tag{4.16}$$

and our final approximation to the sum (4.14) is

$$\sum_{s=0}^{\infty} F_{ts}\psi_s \simeq \sum_{s=0}^{s_o-1} F_{ts}\psi_s + \sum_{p=0}^{m} F_{ts(p)}\psi_{s(p)} w_p(t) \quad . \tag{4.17}$$

The weights $\omega_p(t)$ depend on g/b, but the results for the impedance are virtually insensitive to changes of g/b within the function $\omega_p(t)$; therefore we take an average value (g/b = 2) in ω_p, even though the impedance is calculated for a wide range of g/b.

For the β_p we take cubic splines represented as

$$\beta_p(x) = a_{op} + a_{1p}x + \sum_{q=0}^{m} b_{pq}|x-q|^3 \quad . \tag{4.18}$$

The coefficients a_{op}, a_{1p}, b_{pq} are taken from the tables of Sard and Weintraub.[5] The calculations reported in Section 6 were done with m = 10, and with 10 low modes ($s > s_o$) not treated by splines. Since p = 10 corresponds to $s = \infty$, and $F_{t\infty}\psi_\infty = 0$, we then have 20 mode amplitudes. The infinite-dimensional equations (3.18), (3.19) have

been approximated as 20 equations in 20 unknowns. The sums (4.16), which converge absolutely at a roughly cubic rate, are computed once for all with 5000 terms retained. Modes of even and odd parity decouple, so that only modes with the same parity as the resonant mode enter the calculation.

A test a posteriori to see if our procedure is reasonable is to solve the approximated version of (3.18) or (3.19) and then see whether the solution is consistent with the hypothesis that the function approximated by splines is slowly varying. In the case of (3.18) that means that $A_s(s + a)^{1-\varepsilon}$ should vary slowly over the spline knots $s(p)$, $p = 0, 1, \ldots, m - 1$, since we already know by an independent check that $\tilde{F}_{st}/F^R_{st}$ is almost constant. With $a = 50$, $\varepsilon = 0.1$ (the values used in Section 6), the variation of $A_s(s + a)^{1-\varepsilon}$ and $B_s(s + a)^{1-\varepsilon}$ is indeed agreeably mild, as shown in the example of Table 1. The quantities of Table 1 should tend slowly to zero as $s \to \infty$ (with a behavior differing from $s^{-\varepsilon}$ by an arbitrarily small power) and the data seem to be consistent with that tendency.

(4) Bessel Functions

Bessel functions of complex argument are computed by power series at small argument and asymptotic series at large argument. Bessel function evaluation is not an important factor in the total computation time.

(5) Estimate of Accuracy

There are two issues concerning accuracy:

(i) Are the equations themselves physically correct for the model studied?

(ii) Have the equations been solved with sufficient accuracy?

Regarding (i), we recall that our only approximation in applying Maxwell's equations was the use of the standard resistive wall boundary condition. The latter entails the assumption that fields within the conductor do not vary in a direction parallel to the surface. That assumption may be faulty if the cavity is very short and/or very shallow. In fact we find evidence that our equations are inconsistent with Maxwell's equations in such a case; namely, when both $2g/d \lesssim .1$ and $b/d \gtrsim .7$, with $\sigma_e < \infty$. See the discussion at the end of Section 6. The resistive wall boundary condition appears to be adequate in almost all cases of interest, since the difficulty occurs only in a parameter region where the impedance is very small.

With regard to item (ii), we believe that the only potential source of significant error in solving our equations is the treatment of high coupled modes. To judge that error, we have tried dropping all the modes beyond the 10th (of a given parity), which is to say the infinite set of modes treated by the method of item (3) above. The resulting change in the impedance is so small (less than 0.5% at maxima of impedance) that it would hardly show up in the graphs as plotted in Section 6. Table 1 shows the corresponding small change in the first ten components of the solutions A, B of the (3.18), (3.19). Similarly, changing the way of treating the high modes (changing the mapping, etc.) has negligible effect. Our rather elaborate method was motivated by the observation that the high modes do not decrease very rapidly with mode number. In spite of that, and somewhat surprisingly, their cumulative effect appears to be much less than that of the first few modes.

A convincing check against gross errors is provided by runs with $\sigma_e = \infty$, which can be compared with results of Keil and Zotter[2] obtained by quite a different route. We reproduce the curves of their Figure 4, almost to the accuracy with which we are able to read the curves. The Keil-Zotter curves were computed with 10 cavity modes.

(6) Computation Time

With only the first ten modes retained, computation of all quantities (impedance, frequency, Q factor) for one choice of geometrical parameters and five velocities takes about 3.2 sec of CPU time on a VAX 11/780. Doubling the number of modes triples the time. We have solved (3.18) and (3.19) by iteration, which usually requires six or seven steps for a single-precision solution. The resulting impedance differs little from that obtained with zeroth-order iterates for A and B; one could save time by using the latter.

5. DEPENDENCE OF IMPEDANCE ON PARAMETERS: GENERAL FEATURES

The equations for the impedance entail the following parameters:

a = beam radius

b = tube radius

d = cavity radius

$2g$ = cavity length

R = "ring radius" ($2\pi R$ = longitudinal spatial period)

βc = average particle velocity

(σ_c, σ_t) = conductivity of cylindrical surface of (cavity, tube)

σ_e = conductivity of planar cavity end wall

There are scaling laws and other features which simplify the task of describing the parameter dependence . We must distinguish the resonant impedance Z_c and the smooth-tube impedance Z_t. We discuss only Z_c as described at resonance by the three quantities (3.21), in the mode n given by (3.22). The tube impedance Z_t will be taken up in Part III. The general properties of Z_c may be summarized as follows:

(a) All quantities are independent of R if R is appreciably bigger than d (say $R \gtrsim 5d$). Henceforth we suppose that R/d is indeed large.

(b) The resonant frequency in dimensionless form, $f = (\mathrm{Re}\,\omega_r)d/c$, depends only on g/d and b/d.

(c) If $\sigma = \sigma_c = \sigma_t = \sigma_e$, then $Q(Z_o\sigma d)^{-1/2}$ depends only on g/d and b/d.

(d) If $\sigma = \sigma_c = \sigma_t = \sigma_e$, then $Z_c(\omega = \mathrm{Re}\,\omega_r) \cdot (Z_o\sigma d)^{-1/2}$ depends only on g/d, b/d, and a/d for a fixed value of β. [Usually

the dependence on a/d is negligible, however, since it enters only in the factor $I_1(\chi_n a)/\chi_n a$ which is normally close to its small-a asymptote of 1/2. This factor differs from 1/2 only for very small β and/or unusually large a.]

(e) Aside from the a-dependent factor just mentioned, the β dependence resides entirely in the Bessel function factor,

$$\frac{1}{I_o^2(\chi_n b)} \quad , \tag{5.1}$$

and in the numerator function of the pole term,

$$N = [\tilde{N}_{rn} + \sum_{s\neq r} \tilde{F}_{rs} A_s] \cdot [N_{nr}(1-\eta_t v_r R_r^{-1}) + \sum_{s\neq r} N_{ns}(1-\eta_t v_s R_s^{-1}) B_s] \quad . \tag{5.2}$$

The latter may be approximated by the transit time factor squared: $N \approx |N_{nr}(\kappa = 0)|^2$. The approximation ranges from excellent at small b/d to rather crude at large b/d; it is good enough for practical purposes in most cases (see Section 6 for quantitative details) and in any case we have the useful inequality $N < |N_{rn}(\kappa = 0)|^2$. Thus, the velocity dependence is described in terms of simple explicit factors.

(f) For fixed b/d, the dependence on g/d is similar to that of the small-b impedance given in (2.24), provided that g/d is sufficiently large. This useful fact will be stated more precisely in Section 6, and will be used to get an approximate formula for the impedance.

Keil and Zotter[2] noted property (a) as a result of their numerical calculation. As we remarked in Part I, the validity of their method

at large R is not obvious, so that the basis of their numerical result is not clear. Using our new form of the kernel E, obtained by a Watson-Sommerfeld transformation, one can easily see that the R dependence falls out at surprisingly small magnitudes of R, and that the method is valid at all R. To illustrate the point, we write the expression for the kernel with resistivities put equal to zero; (that simplifies notation without affecting the issue). By (I-5.18, I-5.10), $E = F + \Delta$ where

$$F_{st} = -(g/b)^2 \sum_{i=1}^{\infty} \frac{1}{(g\mu_i/R)^2+(s\pi/2)^2} \; \frac{1}{(g\mu_i/R)^2+(t\pi/2)^2}$$
$$\times \frac{g\mu_i/R}{\sinh \pi\mu_i} [\cosh \pi\mu_i + (-)^{s+1}\cosh(\pi\mu_i - 2g\mu_i/R)] \quad , \tag{5.3}$$

$$\mu_i = R[(j_{oi}/b)^2 - (\omega/c)^2]^{1/2} \quad . \tag{5.4}$$

The i-th zero of the Bessel function J_o is denoted by j_{oi}. Since R enters the equations only through F, we have only to show that (5.3) becomes independent of R. Now $\omega d/c$ at resonance is of order 1; for instance, in the lowest mode $\omega d/c \approx j_{o1} \approx 2.4$, Consequently, the R dependence appears only in $\pi\mu_i$, within the arguments of the hyperbolic functions. But $\pi\mu_i$ is large compared to 1 if R is very large, $\exp(\pi\mu_i)$ dominates both numerator and denominator of the summand of (5.4), and the R dependence goes away. Numerically we find hardly any change in Z_c between R/d = 5 and R/d = ∞.

Property (b) follows from the equation $\mathcal{D}(\omega) = 0$ which defines the resonant frequency, if we neglect all the small complex terms

proportional to resistivities. Since resistive terms are typically smaller than the non-resistive background by a factor of 10^{-4} or so, the neglect is justified so far as determination of $\mathrm{Re}\,\omega_r$ is concerned.

Property (c) is evident in the b = 0 limit, as (2.24) shows. It is not so easy to see why it should hold at larger b/d, but our calculations show it to be true to high accuracy (say one part in 10^3) even at our largest values of b/d. Since $Z_c(\omega = \mathrm{Re}\,\omega_r)$ is proportional to Q, it is not surprising that (d) holds as well as (c); but again there are additional factors which might have spoiled the result but do not.

That the velocity enters only in the Bessel function factors and in the N function (5.2) is rigorously true, and may be read off from the equations. The fact that N is approximated by the transit-time factor, and the validity of (f), are numerical results that are not obvious from inspection of the equations.

Although we have observed no significant violation of properties (a), (b), (c), (d), it is perhaps prudent to do the calculations with reasonable values of those variables that are alleged not to matter. Thus we take d = 1m, R = 100m, and $\sigma = 10^6 (\Omega\,\mathrm{m})^{-1} \simeq$ (conductivity of stainless steel) for the calculations of Section 6.

6. NUMERICAL RESULTS FOR IMPEDANCE, FREQUENCY, AND Q FACTOR

According to Section 5, the principal parameters required for a global description of the resonant impedance are b/d, g/d, and β. Unless one is interested in a case in which the conductivities of the different parts of the chamber walls have different values, the conductivity need not be considered. To an excellent approximation it appears only in a removable factor if $\sigma = \sigma_c = \sigma_e = \sigma_t$. We indeed take equal conductivities, but note that the case $\sigma_t = \sigma_c \neq \sigma_e$ may be treated approximately by a formula to be given presently.

In Figures 1-41 we plot $Z_c(\omega = \mathrm{Re}\,\omega_r)(Z_o\,\sigma d)^{-1/2}$ as a function of 2g/d for various values of b/d and β. The graphs are computed with the factor $I_1(\chi_n a)/\chi_n a$ put equal to 1/2, its limit for $a \to 0$. This is usually a good approximation; when not the reader may correct by including the exact factor using $\chi_n a$ obtained from (2.3) and (3.22); namely,

$$\chi_n a = \frac{f}{\beta\gamma}\,\frac{a}{d} \tag{6.1}$$

We give results for the cavity mode of lowest frequency (i = 1, r = 0) for $0 < 2g/d < 5$, and for the next higher axial mode (i =1, r = 1) for $0 < 2g/d < 10$. As would be expected from the b = 0 formula (2.24), the relative maxima of the r = 1 impedance are larger than the corresponding maxima for r = 0 when g/d is large (say $2g/d \gtrsim 4$). For smaller g/d the r = 0 mode is larger at maxima.

The oscillations of Z_c as a function of 2g/d may be understood as oscillations of the squared transit time factor (2.26), since the latter

approximates the numerator function N of the impedance as defined in equation (5.2). By (3.22) and (3.21) we have

$$k_n g = \frac{f}{\beta}\frac{g}{d} \tag{6.2}$$

Since f varies slowly with g/d, the oscillation of the transit time factor comes from a nearly sinusoidal variation of $\sin k_n g$ ($\cos k_n g$) with frequency inversely proportional to β. For the r = 0 mode we have $(\sin k_n g/k_n g)^2$ for the squared transit-time factor, and the $(k_n g)^{-2}$ contributes a factor β^2 to the impedance. This explains the β^2 variation at fixed geometrical parameters observed by Keil and Zotter[2] over the interval $.5 < \beta < 1$. At smaller values of β the variation can be very different from β^2, because of the factor $I_o^{-2}(\chi_n b)$. Because of the exponential behavior of $I_0(x)$ at large x ($I_o(x) \sim (2\pi x)^{-1/2} \exp(x)$), (6.1) shows that there is an exponential cut-off of the impedance at small β,

$$\exp\left(-2f\frac{b}{d}\frac{1}{\beta\gamma}\right), \quad \beta \to 0 . \tag{6.3}$$

Consequently the cavity must be fairly deep ($b/d \leqslant .3$) to give an appreciable impedance for β as small as .3. Our graphs of Z_c are for the parameter range β = .3, .5, .7, .9, γ = 30 (β = 0.9988) b/d = .2, .3, ..., .9 but with omission of those choices (large b/d/ small β) for which the maximum of $Z_c(Z_o\sigma d)^{-1/2}$ is less than about 1 ohm. Because there is a γ in (6.1) but not in (6.2), the velocity dependence of the impedance for relativistic beams is almost entirely from $I_o^{-2}(\chi_n b)$. Thus, to get the impedance for any $\gamma \gg 1$ from our

results one merely has to scale the graphs for γ = 30 by the factor

$$\left(\frac{I_o(fb/30d)}{I_o(fb/\gamma d)}\right)^2 \tag{6.4}$$

The appropriate value of f in (6.4) is to be taken from Figure 1.

The r = 1 impedance becomes negligibly small for small g/d. The transition to negligible values becomes sharper and occurs at larger g/d as b/d increases. The cut off has to do with the sharp increase of the r = 1 resonance frequency at small g/d, and with the fact that the derivative of the denominator $\mathcal{D}$ of (3.10) also increases sharply. Because of the large derivative $\mathcal{D}'$ it is relatively hard to locate the resonance frequency near and beyond cut-off. The frequency can be found by using damping[6] in the iteration (4.3) while taking very small steps in g/d. That procedure does not lend itself to automatic parameter variation and plotting, however, so we are led to truncate the curves presented at values of g/d where the computation becomes difficult. The impedance is always negligible beyond the point of truncation.

In Figures 42 and 43 we illustrate the effect on Z_c of putting $\sigma_e = \infty$ while keeping $\sigma_c = \sigma_t < \infty$. With $\sigma_e = \infty$ and γ = 30 our values are comparable to those of Keil and Zotter, which were given for $2g/d \leq 2$; (note that our g is one half of theirs by definition). Our values agree with theirs, essentially to the accuracy with which we are able to read their graphs.

The effect of end-wall resistivity is important, of course more so when the ratio of end-wall area to side-wall area is relatively

large. It does not obey a rule-of-thumb suggested by Keil and Zotter,[2] namely that it could be accounted for roughly by augmenting the cylindrical wall resistivity $1/\sigma_c$ in the ratio of new to old resistive surface areas. For a deep cavity ($b/d \ll 1$) that would mean

$$\frac{1}{\sigma_c} \rightarrow \left(1 + \frac{d}{2g}\right) \frac{1}{\sigma_c} \tag{6.5}$$

By the deep cavity formula (2.24) with $\sigma_e = \infty$, that change of σ_c would give

$$Z_c \rightarrow (1 + d/2g)^{-1/2} Z_c \tag{6.6}$$

whereas the correct change obtained from (2.24) with $\sigma_e = \sigma_c$ is

$$Z_c \rightarrow \frac{1+\delta_{ro}}{1+\delta_{ro}+d/g} Z_c \tag{6.7}$$

In Figures 44-47 we plot the dimensionless resonance frequency $f = (\mathrm{Re}\,\omega_r)d/c$ versus $2g/d$ for various b/d. Again some of the curves are truncated at small g/d; beyond each truncation the impedance is negligible and the frequency is hard to compute.

The reduced Q factor, $Q(Z_o\sigma d)^{-1/2}$, is graphed in Figures 48 and 49. In some cases these curves are cut off at slightly higher values of g/d than the corresponding curves of f. The reason in that $Q(Z_o\sigma d)^{-1/2}$ hits a minimum and then begins to increase sharply with decreasing g/d shortly beyond the truncation point of its graph. Such behavior seems unphysical, and appears to be due to inaccuracy of the

resistive wall boundary condition (I-B.12) when b/d is large and g/d small. In the case of the $r = 0$ mode the behavior is without doubt unphysical, since Q goes to infinity and then becomes negative (Imf changes sign) as g/d goes to zero. In the $r = 1$ mode Q stays positive, but still increases abruptly without apparent physical reason. This phenomenon disappears if we make the cavity end walls perfectly conducting ($\sigma_e = \infty$). That makes the end wall boundary condition rigorously correct, since a perfectly conducting wall cannot support field variations transverse to the wall. On the other hand, if $\sigma_e < \infty$ and the cavity is both shallow and short a significant transverse variation probably exists, but is not allowed in the standard boundary condition that we have employed. The $r = 1$ mode, involving faster field variations than $r = 0$, is probably less compatible with the boundary conditions than $r = 0$; hence the bad behavior of Q should show up at larger g/d as it indeed does. Since the field of the beam is primarily radial, one would expect that the boundary condition on the cylindrical cavity wall would be relatively accurate; indeed, we can retain $\sigma_c < \infty$ without any ill effect.

It would be worthwhile to check our calculations at large b/d by using the formalism based on tube modes rather than cavity modes (namely the impedance formula (I-4.26)), which is more appropriate for shallow cavities. If the same bad behavior of Q for short, shallow cavities were obtained, one could then be rather confident that it is due to crudeness of the boundary condition rather than to a simple mistake in computation. We might add that our cavity mode equation for determining ω_r is difficult to analyze for small g/d and large b/d, since it involves several rapidly varying

functions of those parameters. One needs a better approach to the case of short and shallow cavities, which ought to be provided by the tube mode equations.

To summarize the results given in the graphs, as well as to provide a rough interpolation of the parameter values chosen, we shall now concoct a quasi-analytic representation of the impedance. We wish to study the ratio of Z_c to its small-b value (2.24), but the simple ratio will not be well-behaved, since the zeros of $|N_{nr}|^2$ are slightly displaced from those of its large-b counterpart N. Let us then extract the latter factors and form a dimensionless ratio which we call the "reduced impedance":

$$Z_{red} = \frac{Z_c/N}{Z_c(\text{small } b)/|N_{nr}|^2} \tag{6.8}$$

By definition Z_{red} is independent of velocity, and it has the interesting feature of being roughly constant as a function of g/d when that variable is sufficiently large. Furthermore, that constant is nearly a linearly decreasing function of b/d over a large interval. Pretty closely,

$$Z_{red} = 1.175 - 1.35\,\frac{b}{d} \tag{6.9}$$

$$.2 < b/d < .8$$

The approximation (6.9) is good for $2g/d \gtrsim 1$ in the lowest mode ($i = 1$, $r = 0$) and for $2g/d \gtrsim 3$ in ($i = 1$, $r = 1$). This is seen in the graphs of Z_{red} shown in Figures 50 and 51. Now since N is approximated by $|N_{nr}|^2$, we can apply (6.8) to get the desired

estimate of Z_c,

$$Z_c \approx Z_c(\text{small } b)Z_{red} \tag{6.10}$$

Since $N/|N_{nr}|^2$ is not uniformly close to one, this formula should be used for quantitative estimates only near a maximum of $|N_{nr}|^2$. Notice also that (6.10) is not a completely explicit formula for Z_c, since χ_n and k_n involved in Z_c (small b) must be evaluated at the correct value of $f = f(b/d, g/d)$, not at the value of f for $b = 0$. Interpolation or extrapolation of the graphs of Figures 44-47 should give an adequate estimate of f, however.

The accuracy of (6.10) is illustrated in Figures 52-54, which are computed with the exact value of Z_{red}, not (6.9). Thus, the graphs compare Z_c computed with $|N_{nr}|^2$ replacing N to the exact Z_c. For $r = 0$ the error ranges from about 2% at $b/d = .3$ and $2g/d \approx 1$ to about 40% at $b/d = .7$ and $2g/d \approx 4$. In all cases, including $r = 1$, formula (6.10) gives an upper bound on Z_c, and the largest error (which occurs for b/d and g/d large) is about 50% if $b/d \leq .7$. At the first maximum for $r = 0$ (always the largest value of the impedance for a given b/d) the approximation is always fairly good.

To summarize, from (6.9), (6.10), (2.24), and (2.26), the resonant impedance is given approximately in mode $i = 1$, $r = 0, 1$ near one of its relative maxima as

$$Z_c \simeq (1.175-1.35\,\frac{b}{d})\,\frac{2Z_o g}{\pi d}\,\frac{(2\sigma_c Z_o d)^{1/2}}{(j_{o1}^2+(r\pi d/2g)^2)^{5/4}}\left(\frac{j_{o1}}{J_1(j_{o1})}\right)^2$$

$$\times\,\frac{1}{1+\delta_{ro}+(d/g)(\sigma_c/\sigma_e)^{1/2}}\,\frac{1}{I_o^2(\chi_n b)}\left(\frac{k_n g}{(k_n g)^2-(r\pi/2)^2}\right)^2\begin{pmatrix}\sin^2 k_n g, & r=0\\ \cos^2 k_n g, & r=1\end{pmatrix}$$

$$.2 \leqslant b/d \leqslant .8 \qquad (6.11)$$

$$2g/d \geqslant 1 \quad (r=0) \quad ; \quad 2g/d \geqslant 3 \quad (r=1) \quad .$$

Here $j_{o1} \cong 2.405$ is the first zero of J_o, and $J_1(j_{o1}) \cong 0.519$. The wave numbers χ_n and k_n are determined by (6.1) and (6.2), with f taken from Figures 44-47.

Although (6.11) was derived from the computations with $\sigma_t = \sigma_c = \sigma_e$, further computations show that it holds pretty well for $\sigma_t = \sigma_c \neq \sigma_e$. We shall not attempt to describe the degree of approximation globally, but to give an indication we mention that an increase or decrease of σ_e by a factor of 10 produces a change in Z_{red} less than 1% if b/d = .2, less than 10% if b/d = .5, and less than 30% if b/d = .7, when the aspect ratio 2g/d is of order 1. The frequency f is affected negligibly. The quantity Q_{red}, defined by

$$Q_{red} = Q\,(Z_o\sigma d)^{-1/2}\left(1+\frac{1}{1+\delta_{ro}}\,\frac{d}{g}\left(\frac{\sigma_c}{\sigma_e}\right)^{1/2}\right) \qquad (6.12)$$

undergoes about the same fractional change as Z_{red} when σ_e is varied at fixed $\sigma_t = \sigma_c$. This property is suggested by the small-b formula for Q, Eq. (2.27). Variations due to changing σ_t seem harder to describe. We mention only that for small b/d (say 0.2 or so) it is a good approximation to put $\sigma_t = \infty$ provided $\sigma_t \geq \sigma_c$. Even for

b/d = 0.5, the change in Z_{red} is only about 25%, if we replace $\sigma_t = \sigma_c$ by $\sigma_t = \infty$. Generally speaking, the tube connected to the cavity has a moderate to negligible effect if b/d $\leq$ 0.5, but for b/d > 0.5 its effect increases rapidly.

Formula (6.11) illustrates a fact mentioned in Ref. 2: for very long cavities (2g/d >> 1) the r = 1 impedance is nearly twice the r = 0 impedance. This is a special circumstance arising from the anomalous status of the constant term in a Fourier series, and does not indicate a trend in the behavior of higher modes. At small b/d it follows from (2.24) that higher modes will give a smaller impedance than the two modes we have considered. (It is understood that impedances are evaluated at maxima of transit time factors for comparison of different modes. Of course, at a minimum of the transit time factor for a low mode some higher mode could give a bigger impedance). It seems likely that the same situation holds at large b/d, but we have not studied the question numerically. A difficulty arises in following higher mode solutions as b/d increases. One encounters "tube resonances", which is to say frequencies at which $I_o(\chi_m b) = 0$ for low m, the resonant frequencies of a smooth tube of radius b. This resonance condition is equivalent to $\sinh \pi\mu_m = 0$ in (5.3), which implies the presence of a pole in the kernel matrix F_{st}. (Here we neglect resistivities, which do not effect the essential point). The presence of the pole gives a rapidly varying $\mathcal{D}$, which makes it hard to follow the cavity resonance. At least temporarily the latter is close to the tube resonance; perhaps the two eventually separate as b/d increases. Techniques could be devised to investigate this situation, for instance by using the tube mode equations with a resonant mode elimination like that of Section 3.

7. CONCLUSIONS

In computing the coupling impedance from the cavity mode equations we have demonstrated the value of two techniques: (1) transformation of the kernel matrix of the equations by the Watson-Sommerfeld method (Section 5, Part I); (2) elimination of the resonant mode amplitude (Section 3). Perhaps these methods provide more power than is necessary for the relatively simple problem at hand, but they provide more mathematical and physical insight and easier computational problems than the straightforward approach of solving the original mode equations. More importantly, we believe that similar methods could offer real advantages in more complicated problems, for instance in finding transverse coupling impedances or longitudinal impedances for a cylindrical tube with three or more discontinuities of radius per period. The perturbative method that follows from item (2) above, carried to lowest order, should provide a very simple approximate solution of the relatively complicated equations that would be obtained.

ACKNOWLEDGMENT

We wish to thank Stanley Fenster for introducing us to the problems studied and for many helpful discussions. We also thank the Theoretical Physics Group at Lawrence Berkeley Laboratory for kind hospitality and the use of computer facilities. This work was supported by the Director, Office of Energy Research, Office of High Energy and Nuclear Physics, Division of High Energy Physics of the U.S. Department of Energy under Contract DE-AC03-76SF00098.

REFERENCES

1. R. L. Warnock, G. R. Bart, and S. Fenster, "Longitudinal Stability of a Coasting Beam in a Resistive Vacuum Chamber with Cylindrical Resonant Cavity". Part I: Self Consistent Field Equations and a Method to Improve Convergence", LBL-13180 1/2, to be published in Particle Accelerators.
2. E. Keil and B. Zotter, Particle Accelerators 3, 11 (1972).
3. R. G. Newton, Scattering Theory of Waves and Particles, (McGraw-Hill, New York, 1966); §12.12.
4. L. Collatz, Functional Analysis and Numerical Mathematics, (Academic Press, New York, 1966).
5. A. Sard and S. Weintraub, A Book of Splines, (Wiley, New York, 1971).
6. Divergence of the iterative sequence (4.3) may sometimes be cured by multiplying the second term of (4.3) by a "damping" factor ξ, where $0 < \xi < 1$. For a discussion with references of the analogous damped Newton method see R. L. Warnock, J. Comput. Phys. 33, 45 (1979).

Table 1 Solutions of equations (3.18), (3.19) for $r = 0$, $b/d = .5$, $2g/d = 2$, $\gamma = 30$. Only the real parts are tabulated, the imaginary parts being smaller by a factor of about 10^{-4}. The last two columns are for the case in which the high modes ($s > 20$) are dropped.

s	$(s + a)^{1-\varepsilon}A_s$	$(s + a)^{1-\varepsilon}B_s$	$(s + a)^{1-\varepsilon}A_s$	$(s + a)^{1-\varepsilon}B_s$
2	12.8	1.35	12.8	1.34
4	5.77	2.49	5.74	2.45
6	4.09	2.39	4.05	2.35
8	3.32	2.23	3.26	2.17
10	2.86	2.09	2.79	2.02
12	2.56	1.97	2.48	1.90
14	2.34	1.88	2.26	1.80
16	2.17	1.80	2.09	1.71
18	2.04	1.73	1.95	1.64
20	1.94	1.68	1.84	1.58
23.7	1.79	1.60	-	-
28.2	1.66	1.52	-	-
33.7	1.56	1.46	-	-
40.4	1.46	1.40	-	-
49.0	1.38	1.35	-	-
60.7	1.32	1.30	-	-
77.8	1.25	1.27	-	-
106.	1.20	1.24	-	-
171.	1.17	1.23	-	-
∞	0	0	-	-

FIGURE CAPTIONS

Fig. 1 to Fig. 27: $Z_c \cdot (Z_o \sigma d)^{-1/2}$ in ohms, at resonance, for cavity aspect ratio in the range $0 < 2g/d < 5$. The solid curve is for mode ($i = 1$, $r = 0$), while the dashed curve is for ($i = 1$, $r = 1$). The impedance is for tube mode n given by (3.22).

Fig. 28 to Fig. 41: $Z_c \cdot (Z_o \sigma d)^{-1/2}$ in ohms, at resonance , for cavity aspect ratio in the range $5 < 2g/d < 10$. Both curves on each graph are for mode ($i = 1$, $r = 1$), the higher one being for the lower of the two values of b/d indicated. The impedance is for tube mode n given by (3.22).

Fig. 42 to Fig. 43: The effect of cavity end wall resistance on the impedance. The solid curve is with end wall resistance, the dashed curve without.

Fig. 44: The dimensionless resonant frequency $f = (\mathrm{Re}\,\omega_r)d/c$ for the lowest mode ($i = 1$, $r = 0$). Ordered from top to bottom, the five curves are for b/d = .2, .3, .4, .5, .6.

Fig. 45: The dimensionless resonant frequency $f = (\mathrm{Re}\,\omega_r)d/c$ for the lowest mode ($i = 1$, $r = 0$). The three curves (solid,dashed, dot-dashed) are for b/d = .7, .8, .9, respectively.

Fig. 46: The dimensionless resonant frequency $f = (\mathrm{Re}\,\omega_r)d/c$ for the mode ($i = 1$, $r = 1$). Ordered from top to bottom, the five curves are for b/d = .2, .3, .4, .5, .6.

Fig. 47: The dimensionless resonant frequency $f = (\mathrm{Re}\,\omega_r)d/c$ for the mode ($i = 1$, $r = 1$). The three curves (solid, dashed, dot-dashed) are for b/d = .7, .8, .9, respectively.

Fig. 48: The reduced Q factor, $Q(Z_o \sigma d)^{-1/2}$, for mode ($i = 1$, $r = 0$). Ordered from top to bottom, the eight curves are for b/d = .9, .8, .7, .6, .5, .4, .3, .2.

Fig. 49: The reduced Q factor, $Q(Z_o\ d)^{-1/2}$, for mode ($i = 1$, $r = 1$). Ordered from top to bottom, the eight curves are for b/d = .9, .8, .7, .6, .5, .4, .3, .2.

Fig. 50: The dimensionless "reduced impedance" Z_{red}, defined in Eq. (6.8), for mode ($i = 1$, $r = 0$). Ordered from top to bottom, the eight curves are for b/d = .2, .3, .4, .5, .6, .7, .8, .9.

Fig. 51: The dimensionless "reduced impedance" Z_{red}, defined in Eq. (6.8), for mode ($i = 1$, $r = 1$). Ordered from top to bottom, the eight curves are for b/d = .2, .3, .4, .5, .6, .7, .8, .9. All of the curves drop abruptly in some region as g/d is decreased. We have not plotted that region for the top four curves.

Fig. 52 to Fig. 54: A comparison of the exact impedance (solid curve) with that computed from the approximation $N \simeq |N_{nr}|^2$ (dashed curve). The two curves represent the left and right sides, respectively, of Eq. (6.10), if the exact value of Z_{red} is used. Notice that the approximation gives an upper bound for the impedance.

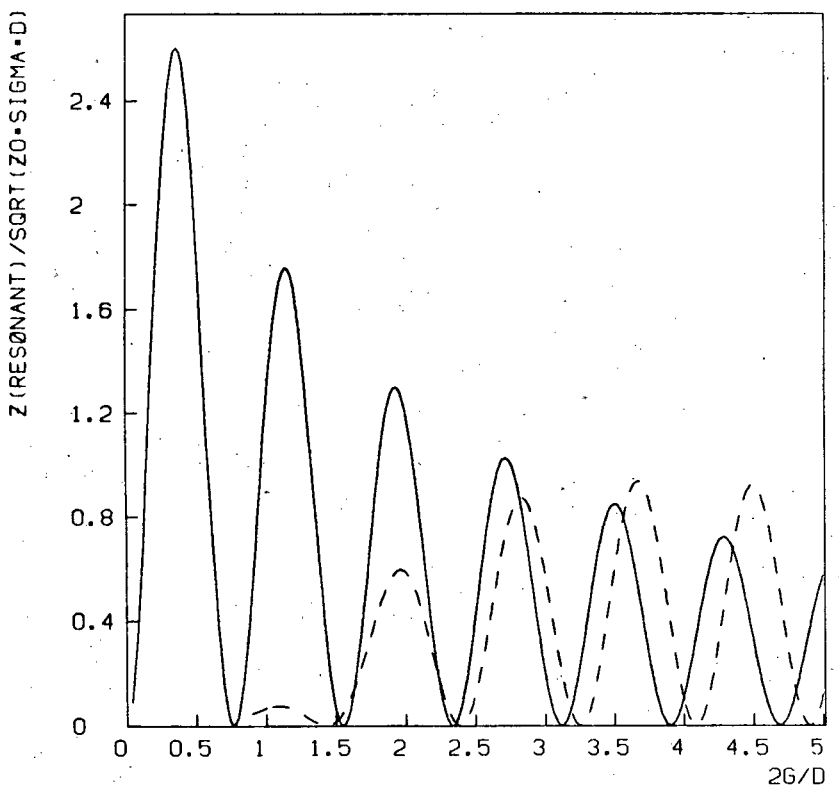

FIG.1 BETA=.3 B/D=.2

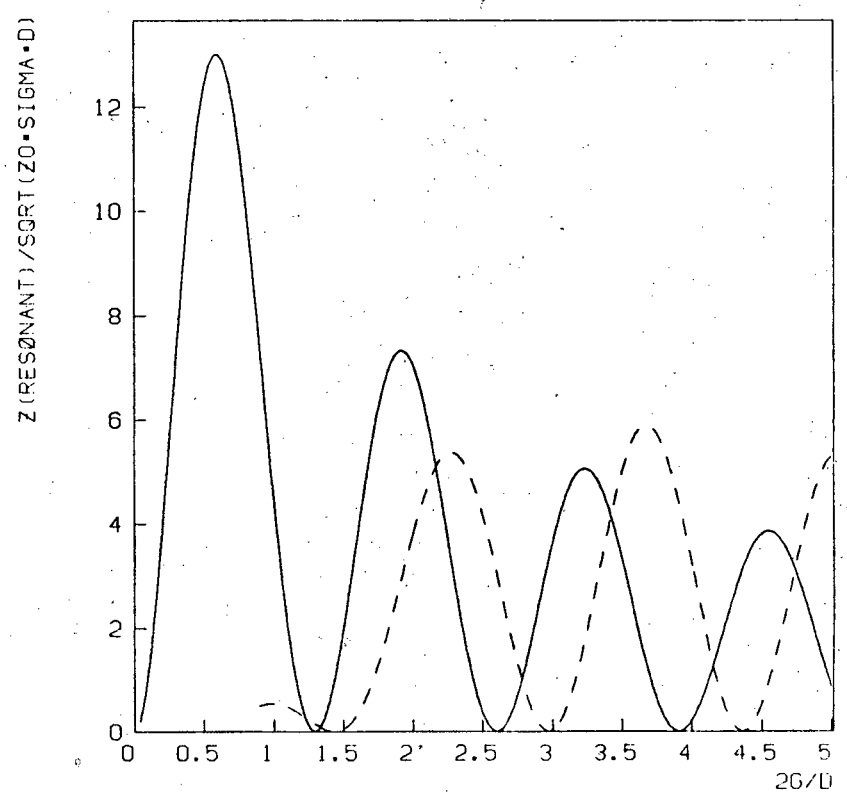

FIG.2 BETA=.5 B/D=.2

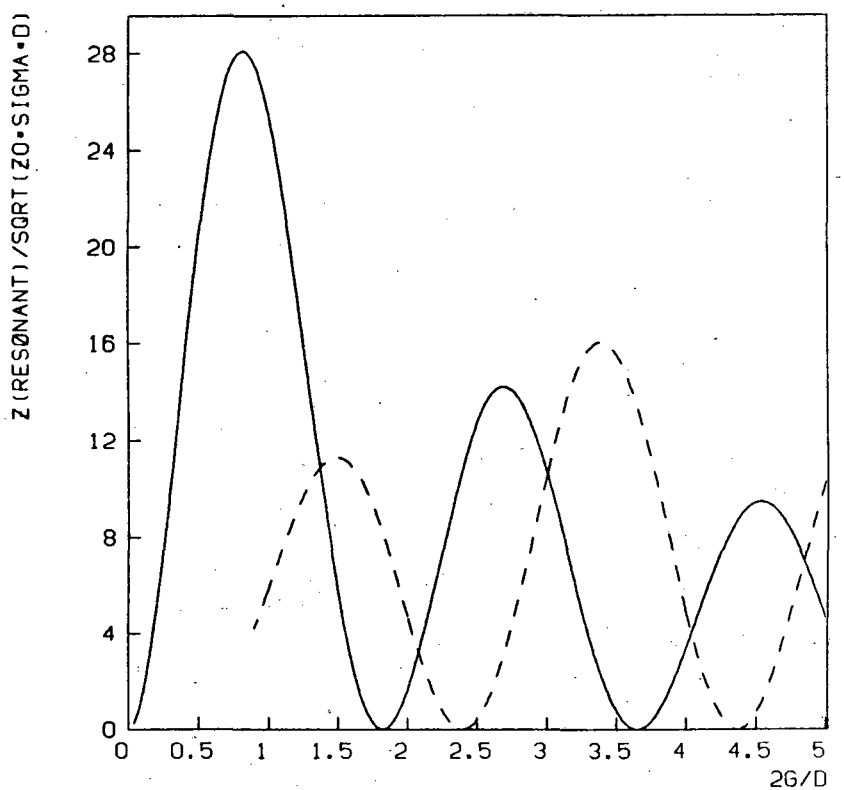

FIG.3 BETA=.7 B/D=.2

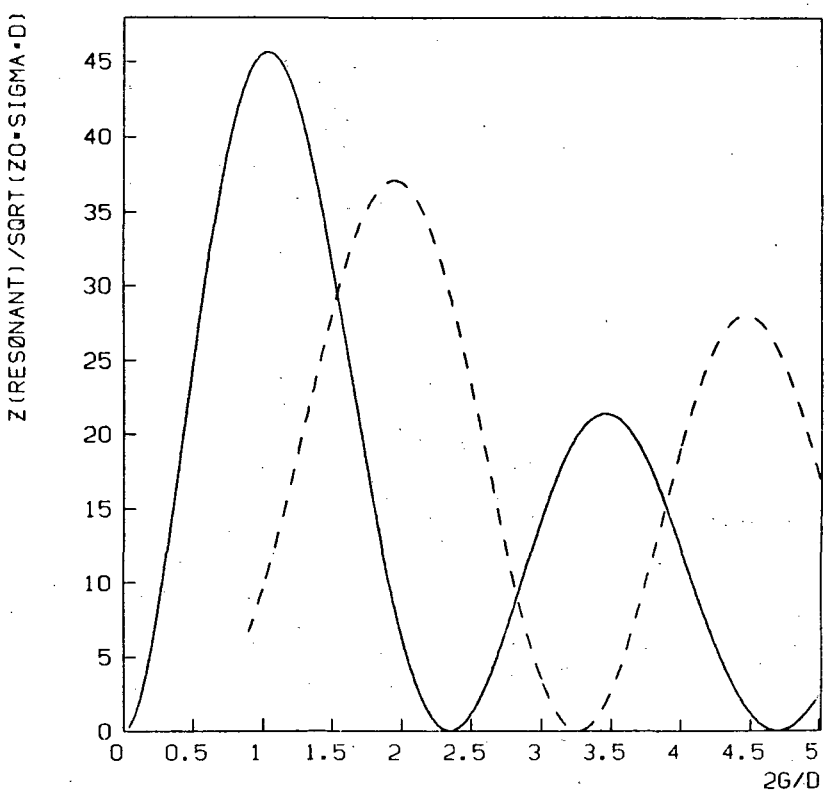

FIG.4 BETA=.9 B/D=.2

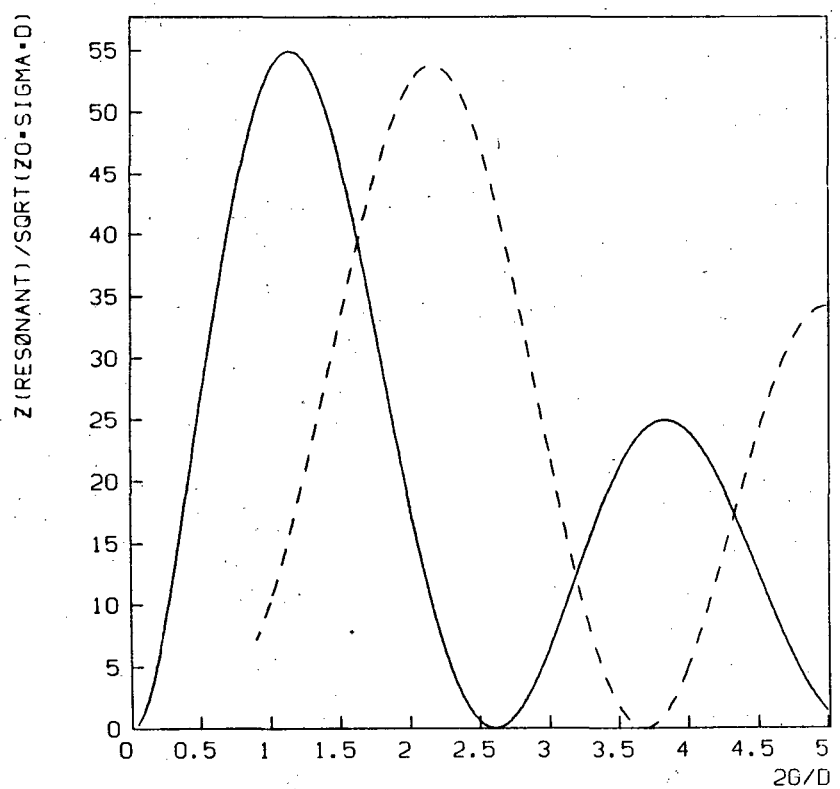

FIG.5 GAMMA=30 B/D=.2

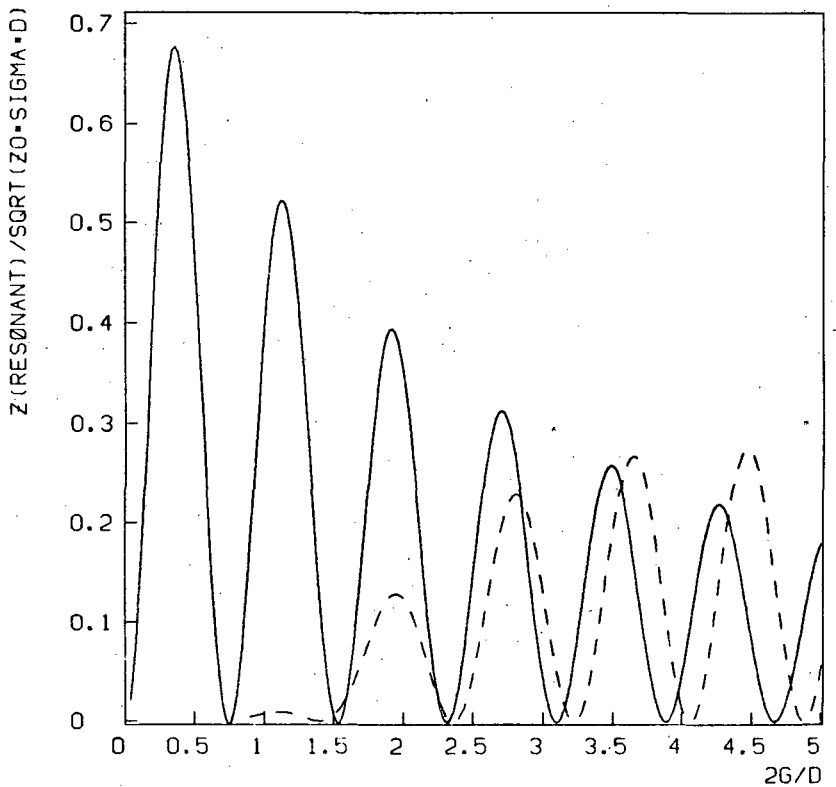

FIG.6 BETA=.3 B/D=.3

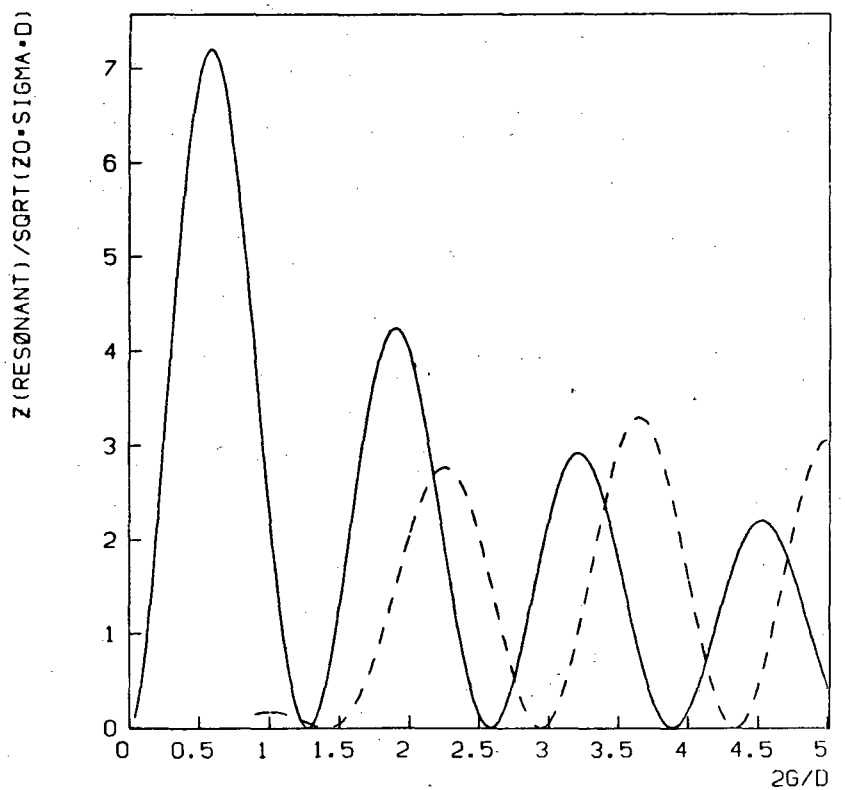

FIG.7 BETA=.5 B/D=.3

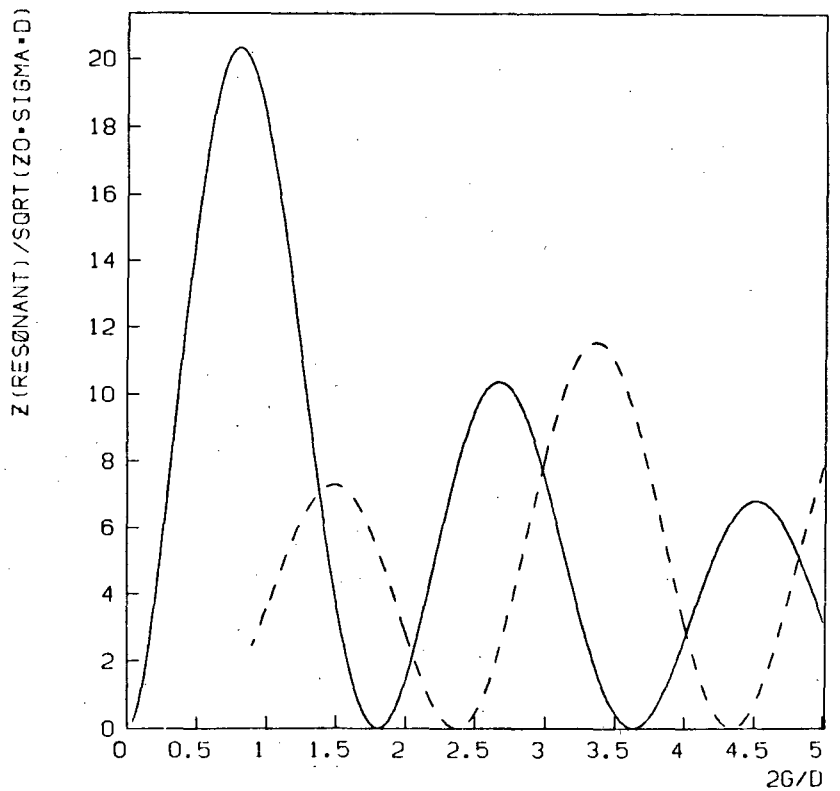

FIG.8 BETA=.7 B/D=.3

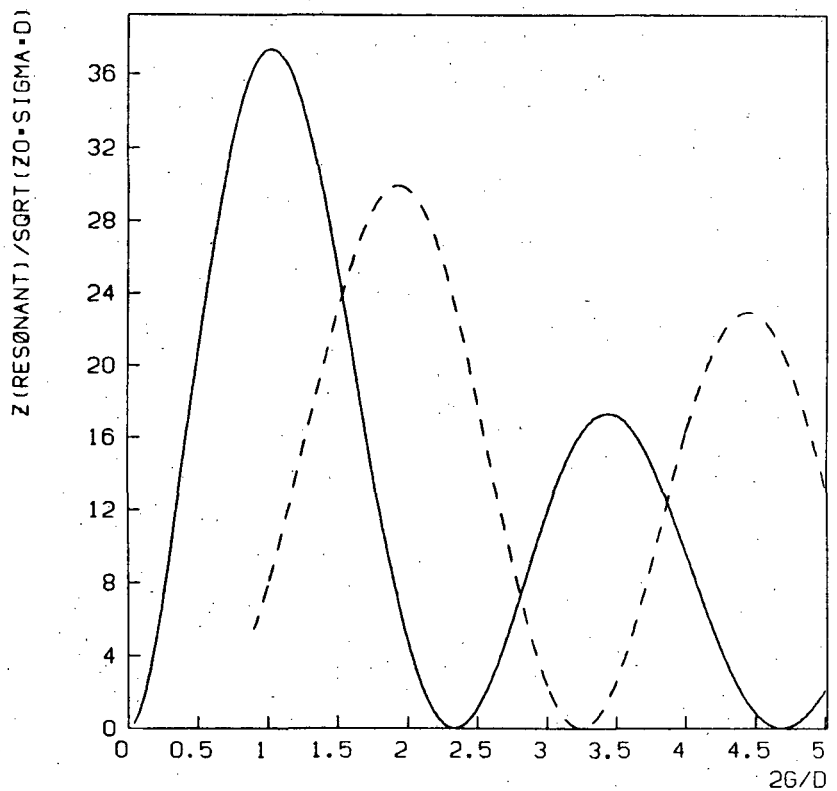

FIG.9 BETA=.9 B/D=.3

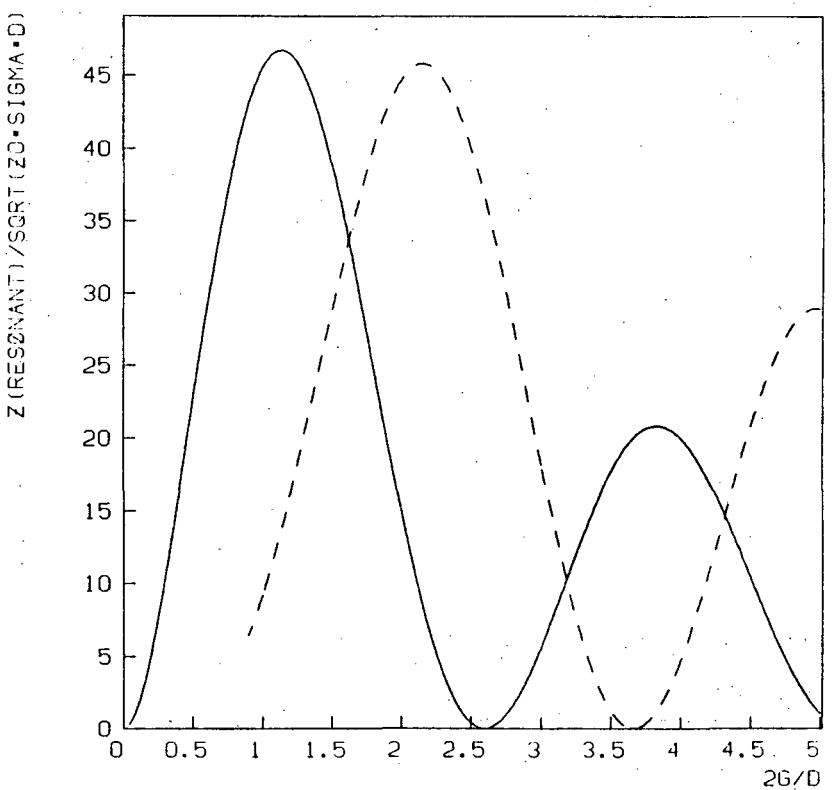

FIG.10 GAMMA=30 B/D=.3

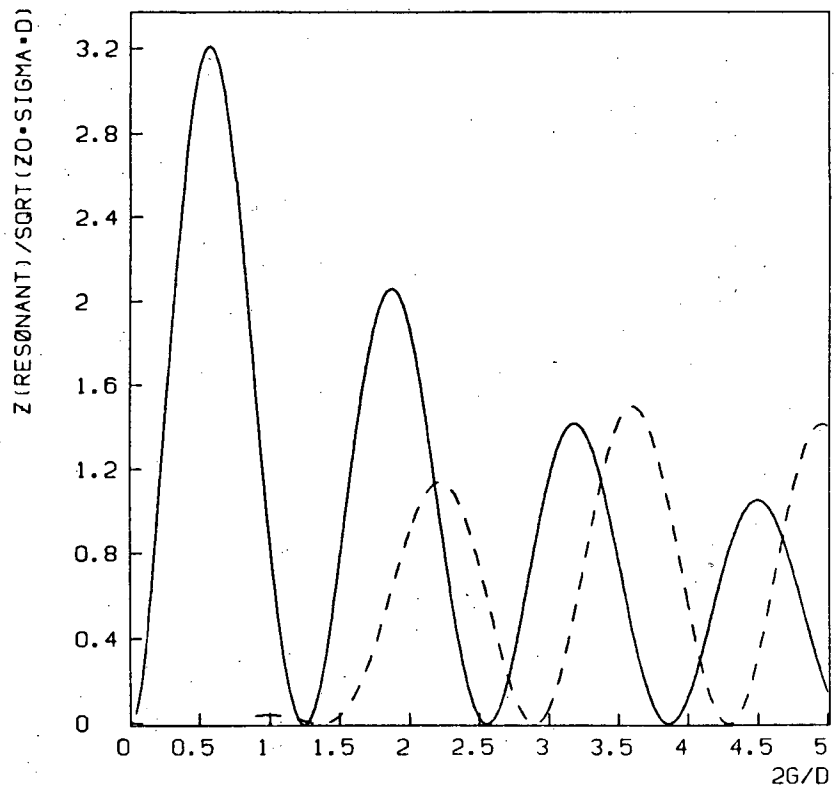

FIG.11 BETA=.5 B/D=.4

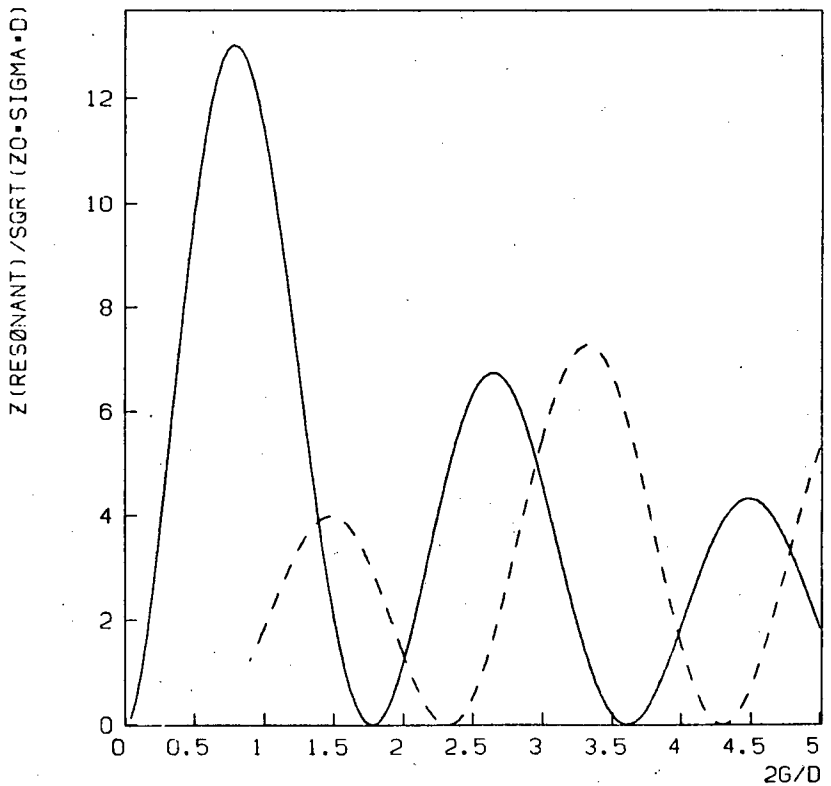

FIG.12 BETA=.7 B/D=.4

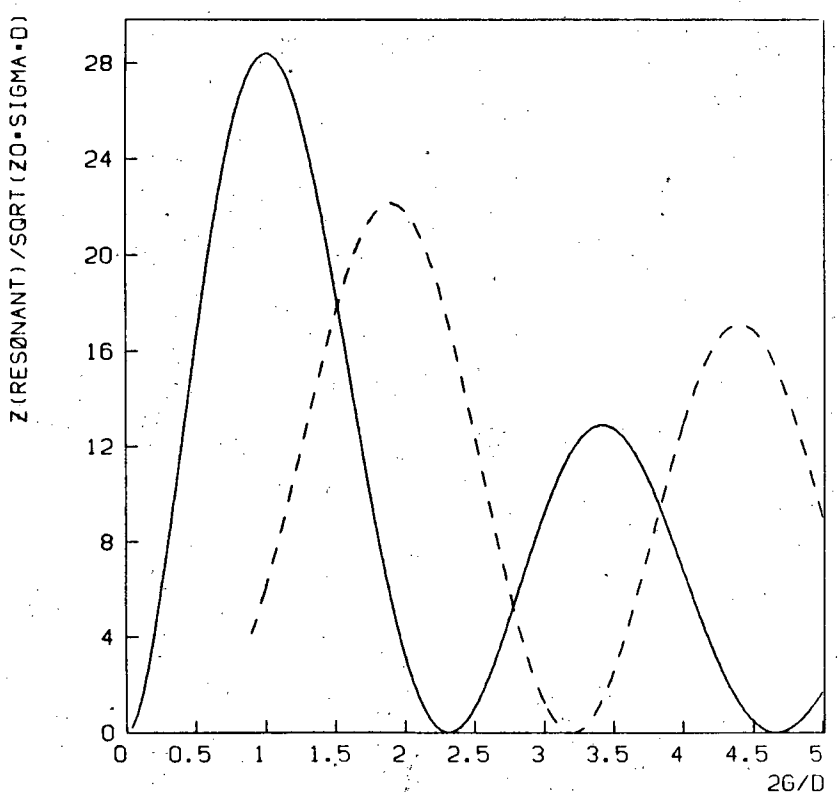

FIG.13 BETA=.9 B/D=.4

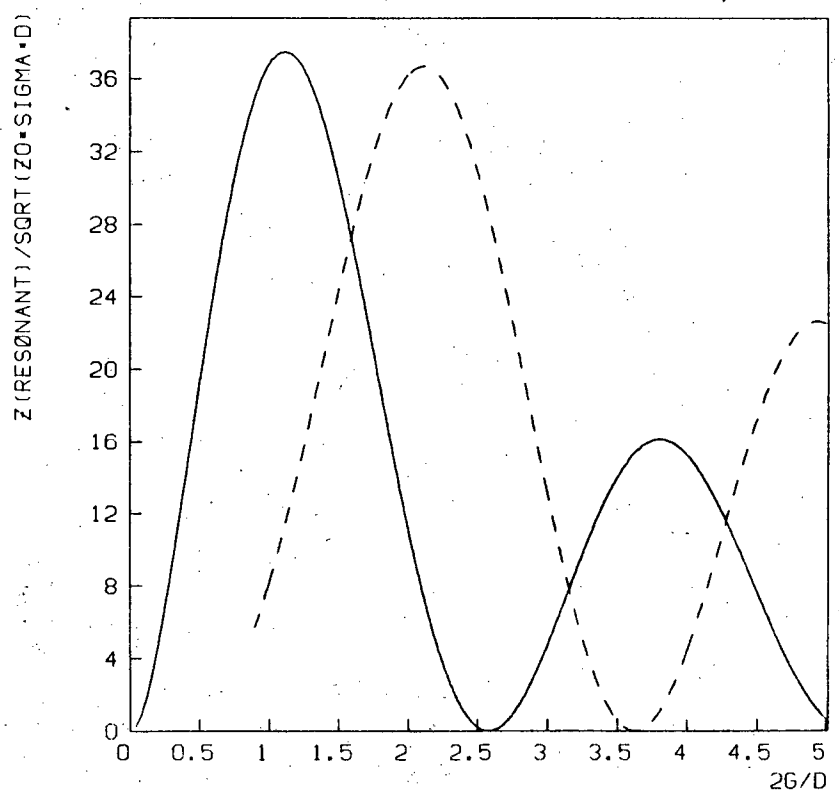

FIG.14 GAMMA=30 B/D=.4

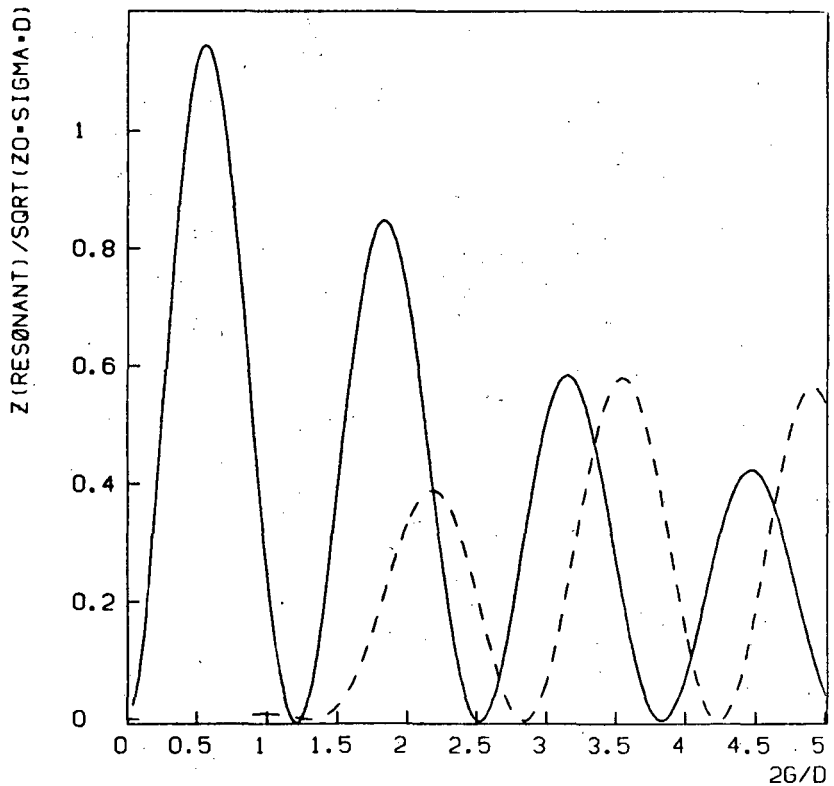

FIG.15 BETA=.5 B/D=.5

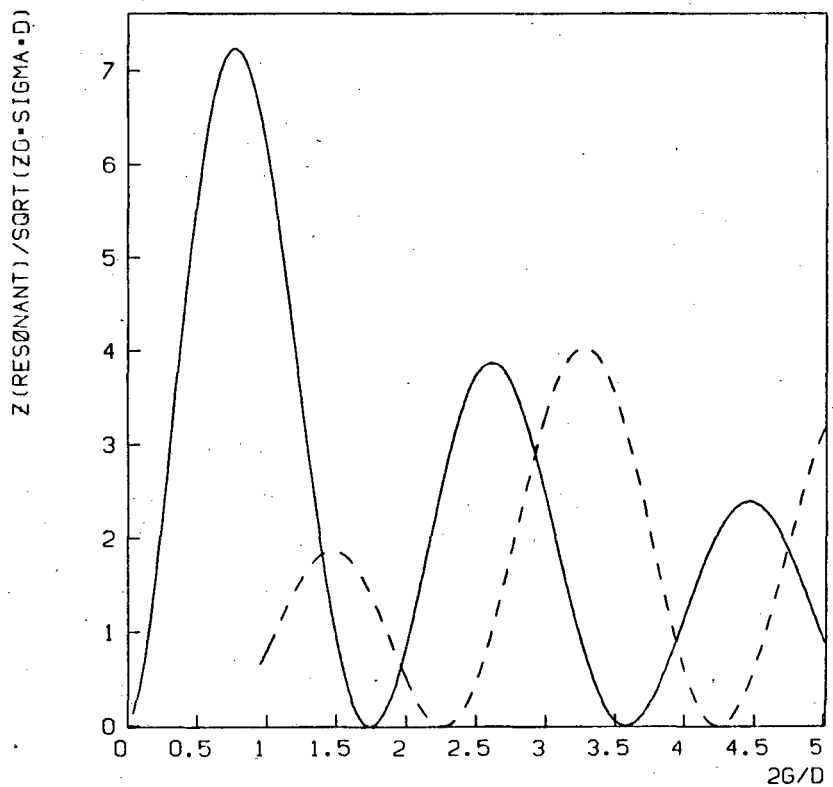

FIG.16 BETA=.7 B/D=.5

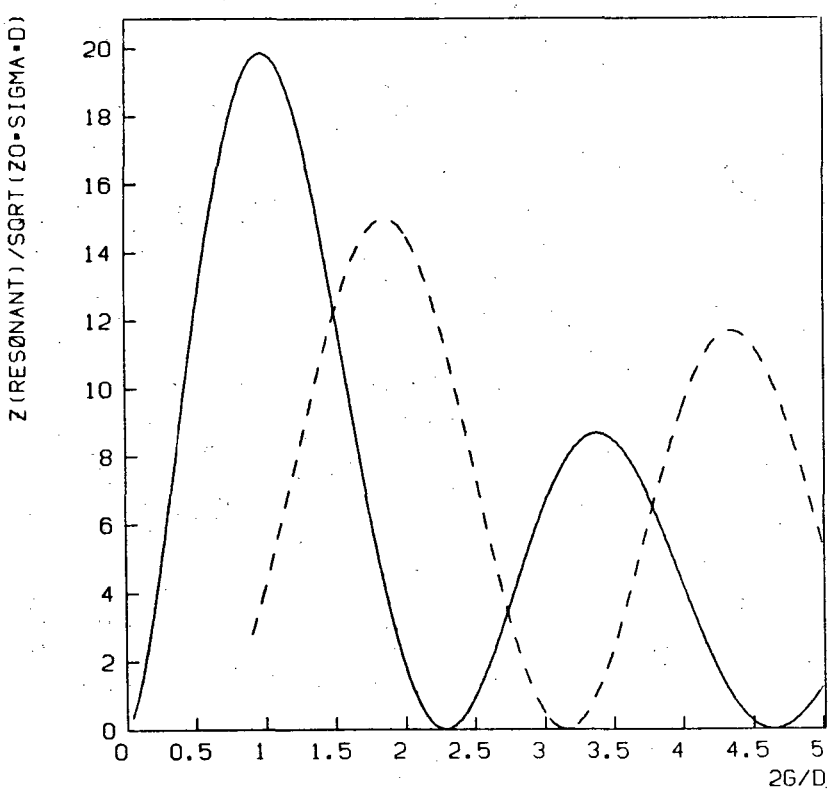

FIG.17 BETA=.9 B/D=.5

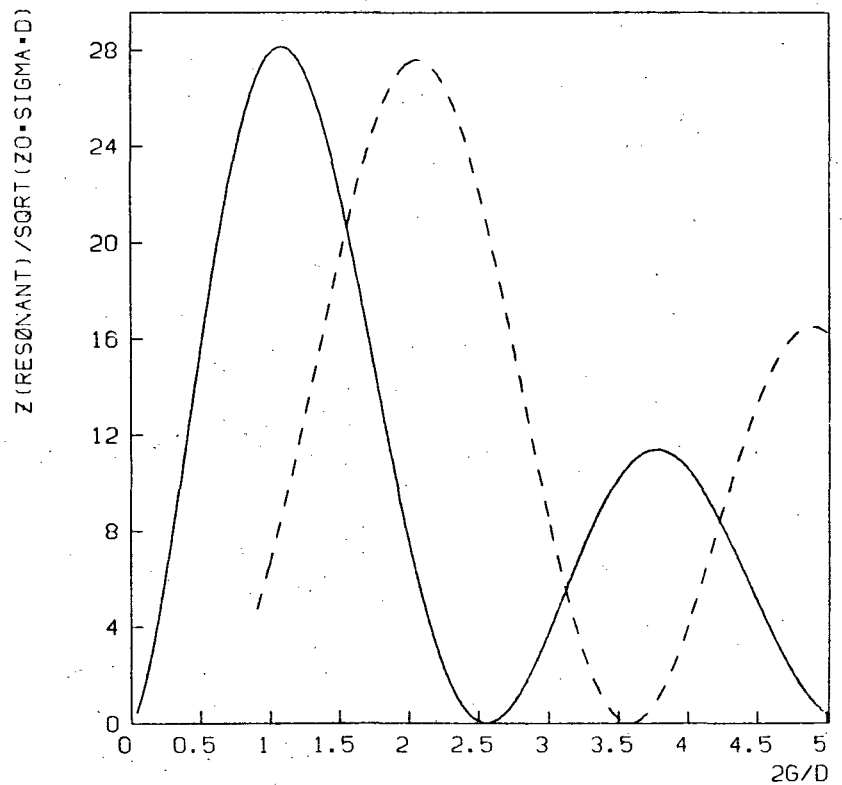

FIG.18 GAMMA=30 B/D=.5

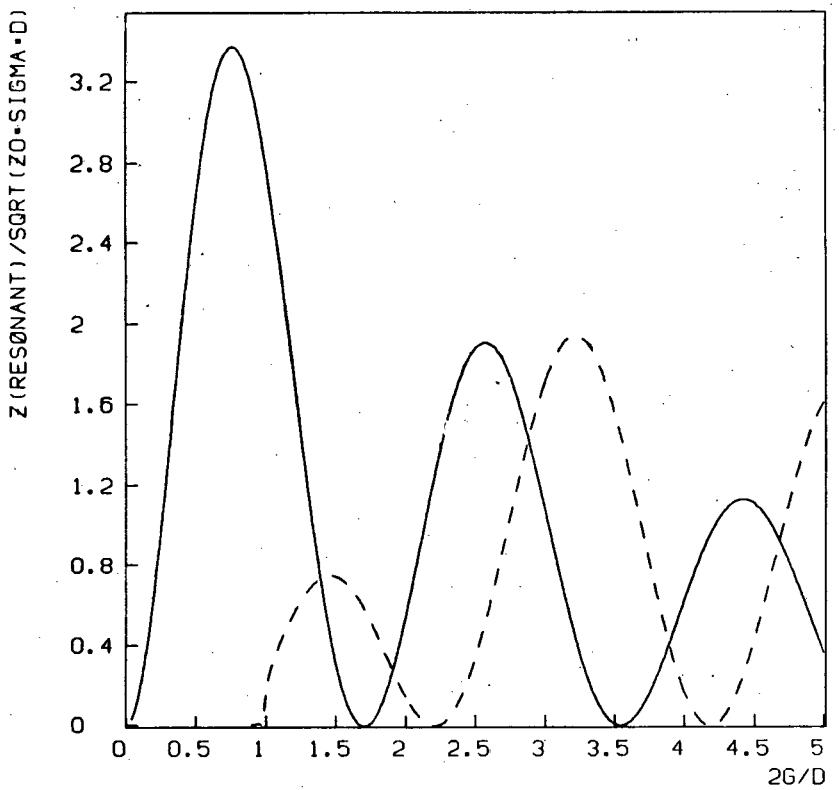

FIG.19 BETA=.7 B/D=.6

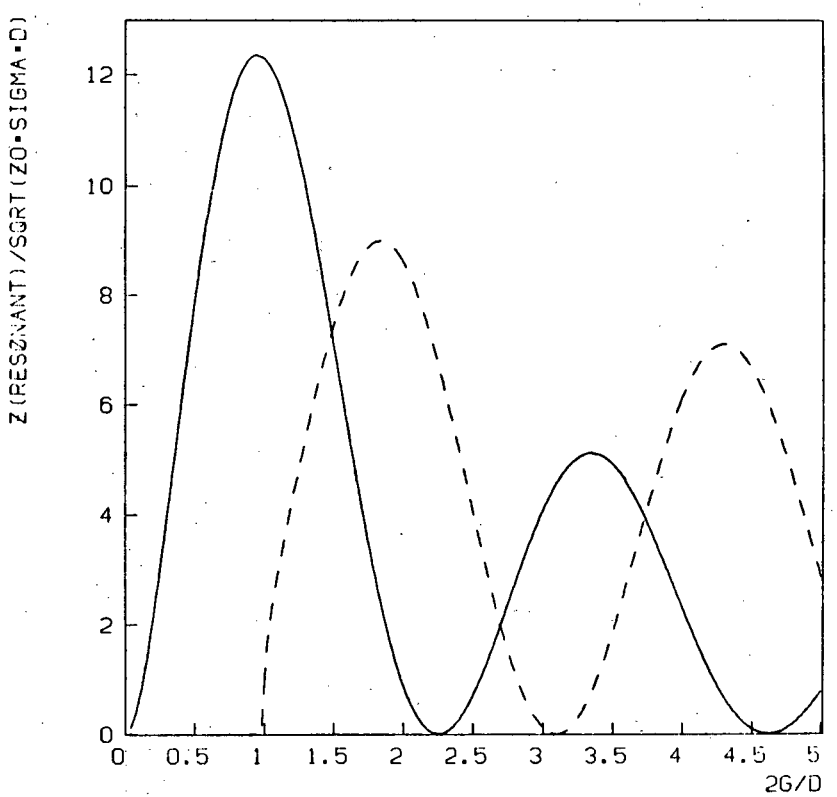

FIG.20 BETA=.9 B/D=.6

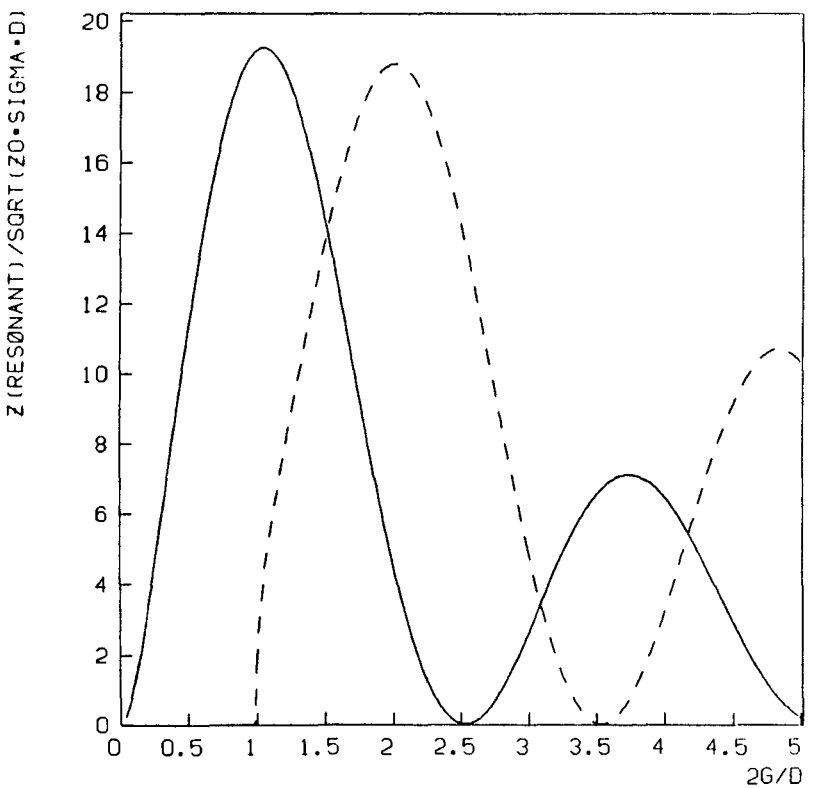

FIG.21 GAMMA=30 B/D=.6

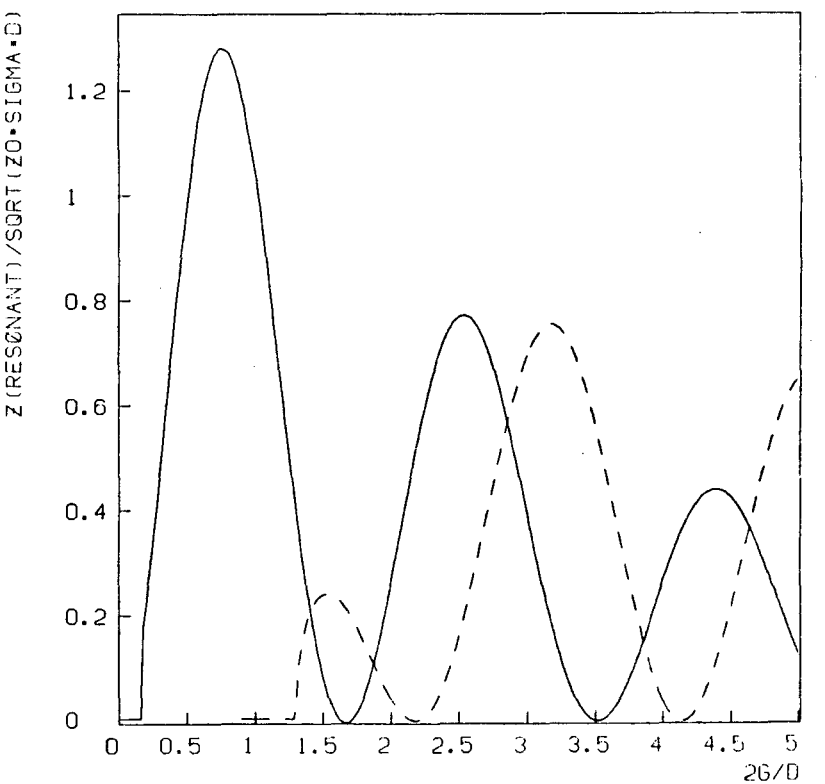

FIG.22 BETA=.7 B/D=.7

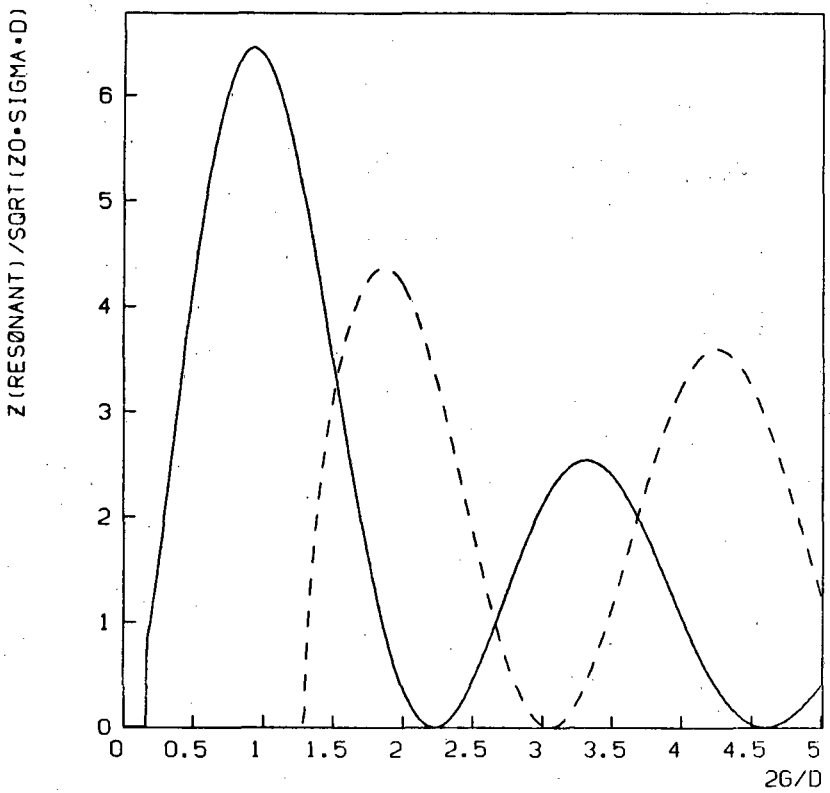

FIG.23 BETA=.9 B/D=.7

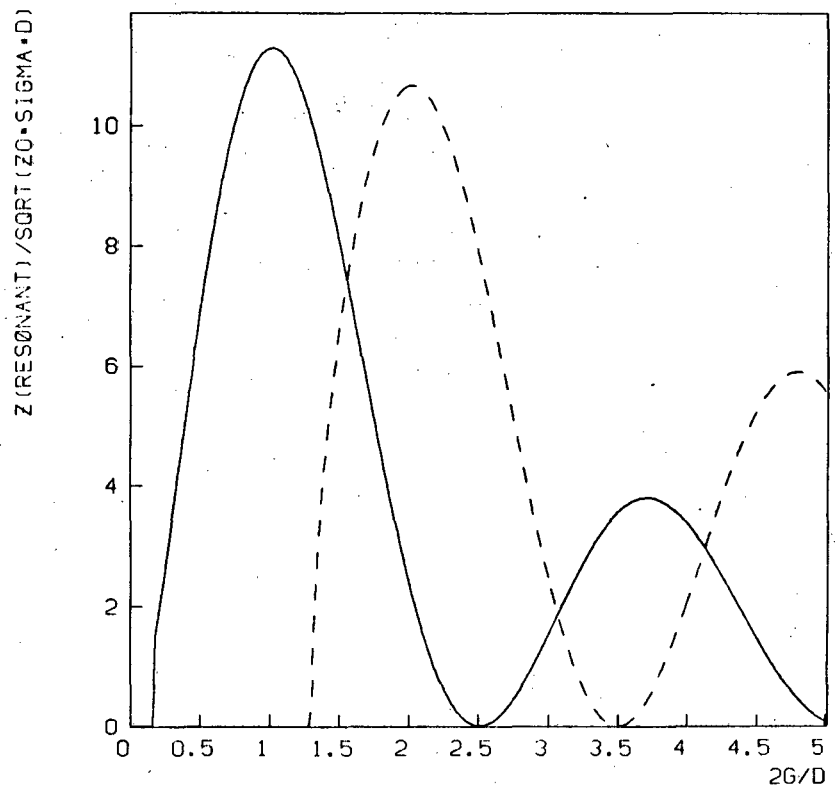

FIG.24 GAMMA=30 B/D=.7

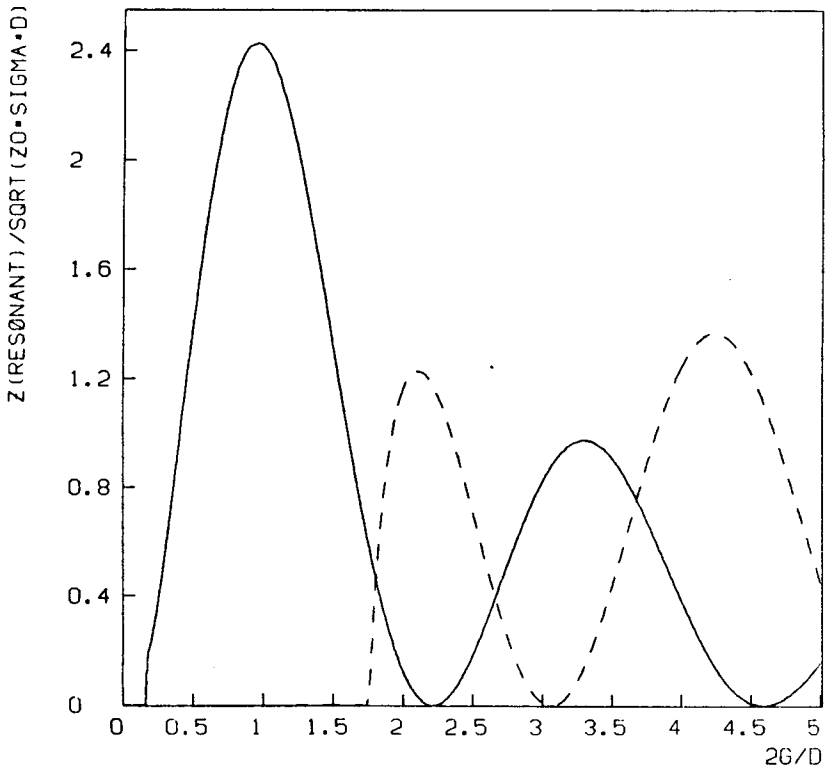

FIG.25 BETA=.9 B/D=.8

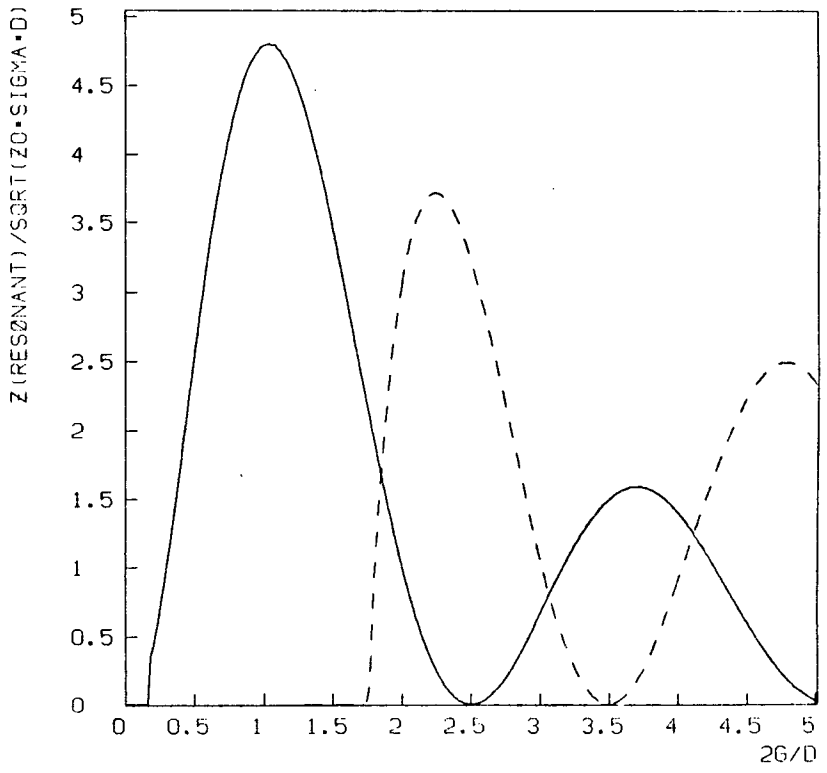

FIG.26 GAMMA=30 B/D=.8

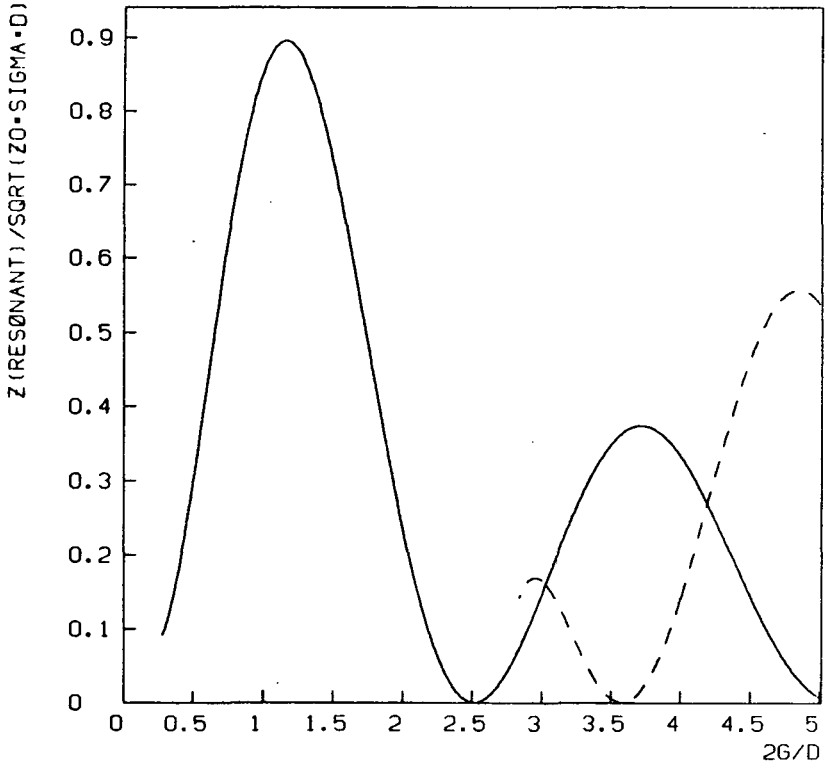

FIG.27 GAMMA=30 B/D=.9

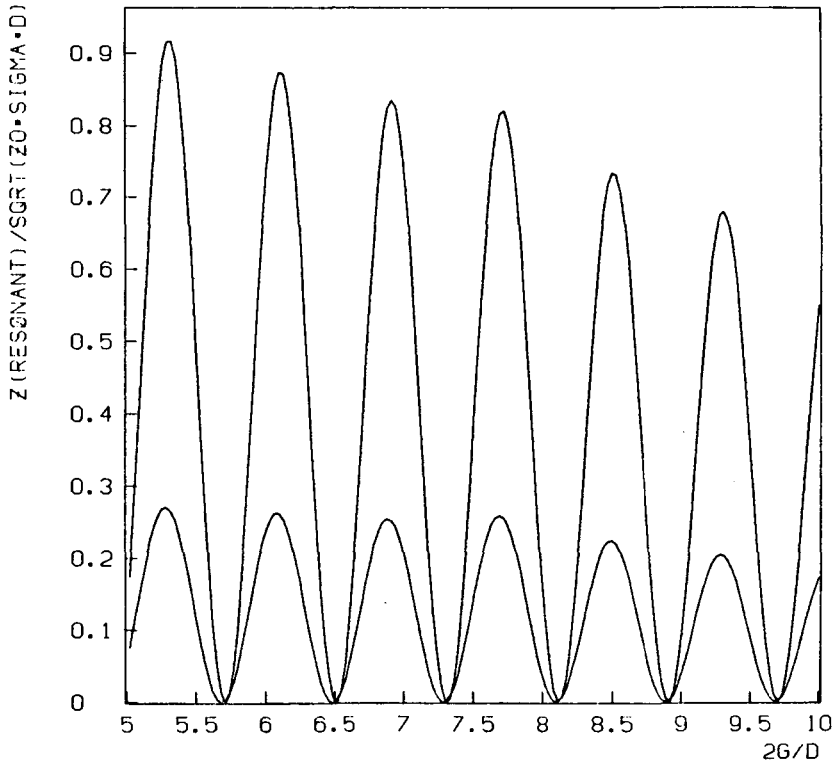

FIG.28 BETA=.3 B/D=.2,.3

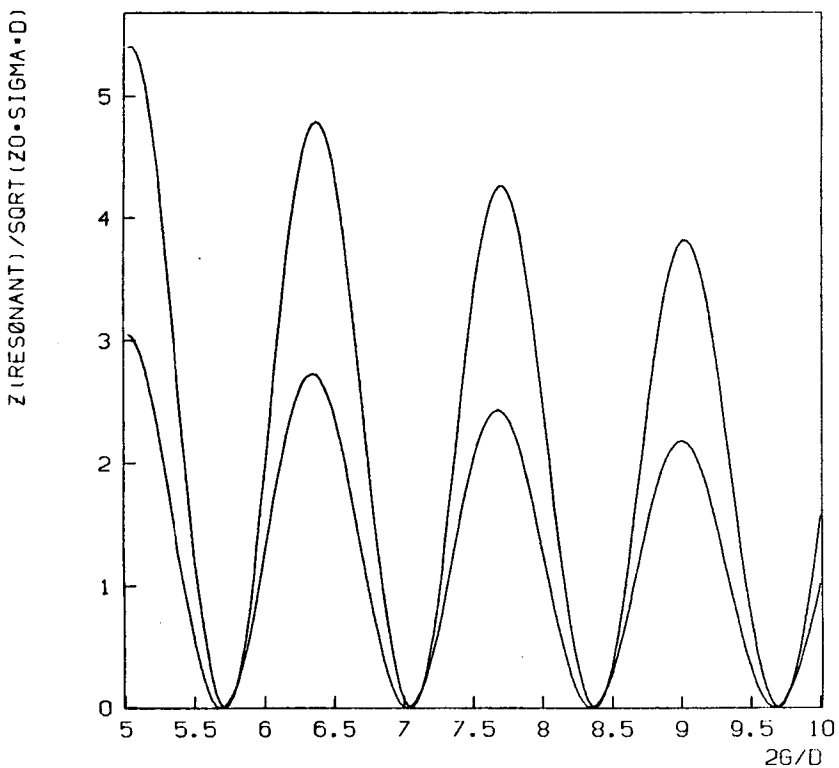

FIG.29 BETA=.5 B/D=.2,.3

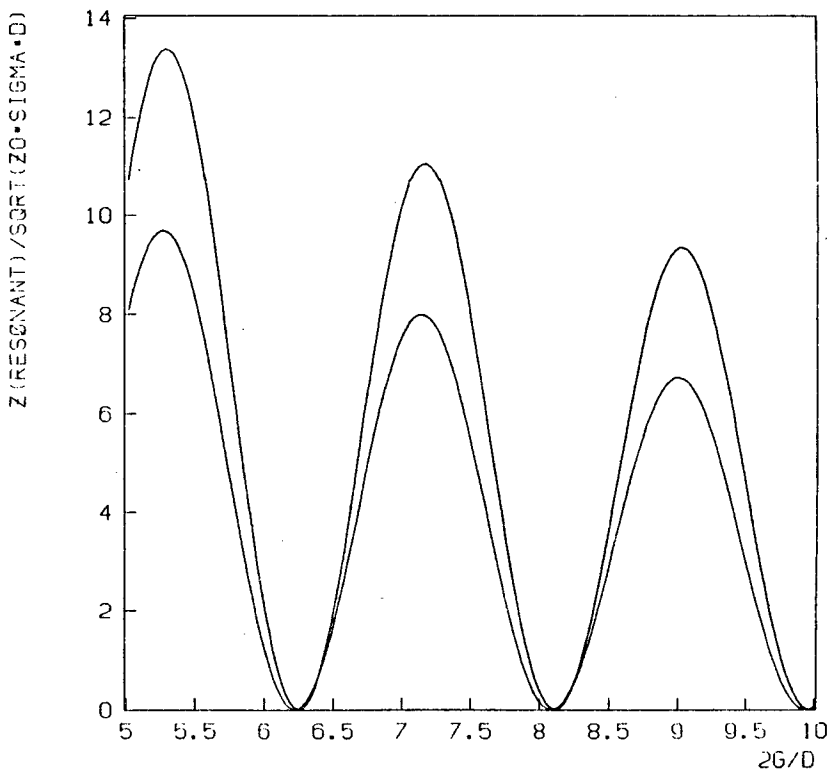

FIG.30 BETA=.7 B/D=.2,.3

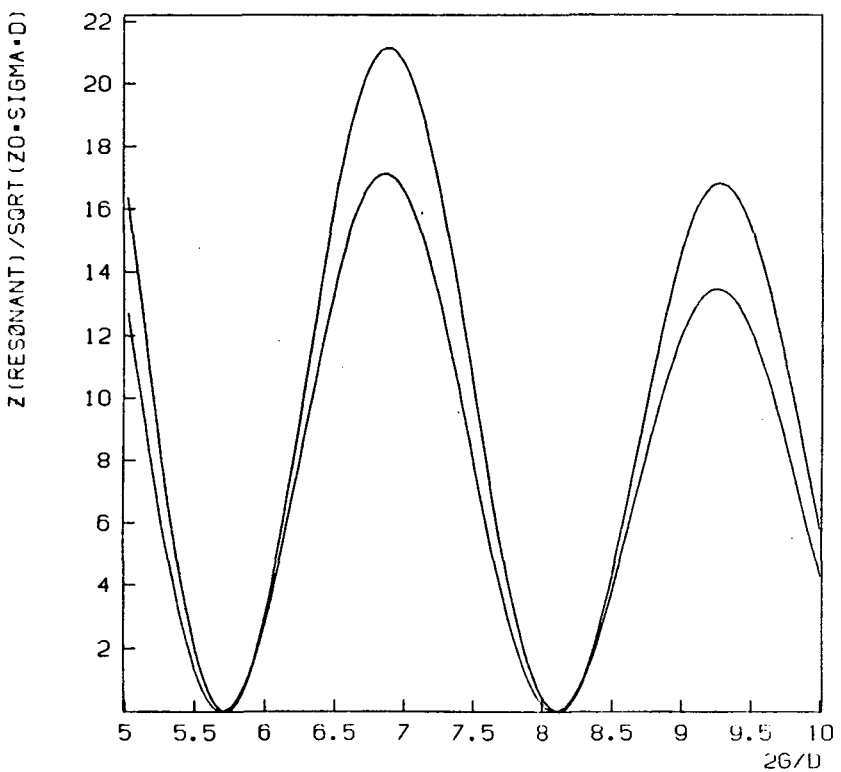

FIG.31 BETA=.9 B/D=.2,.3

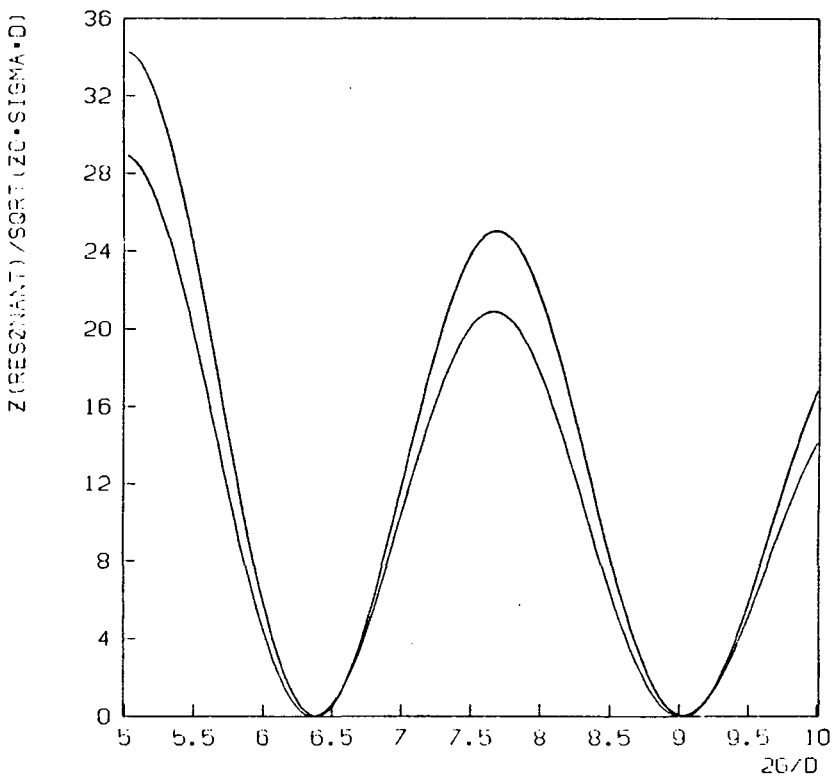

FIG.32 GAMMA=30 B/D=.2,.3

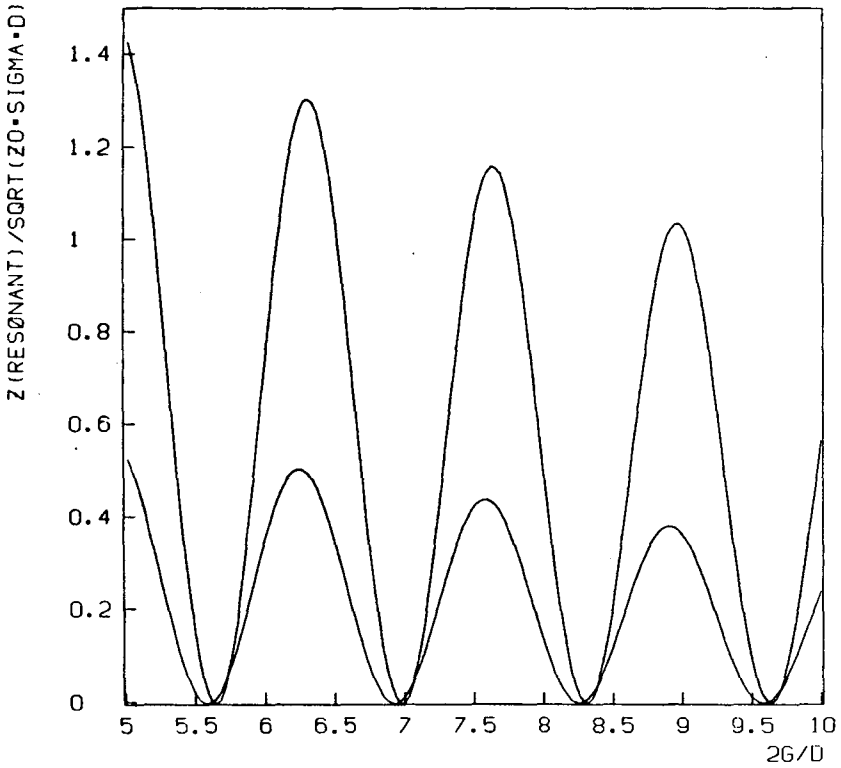

FIG. 33 BETA=.5 B/D=.4,.5

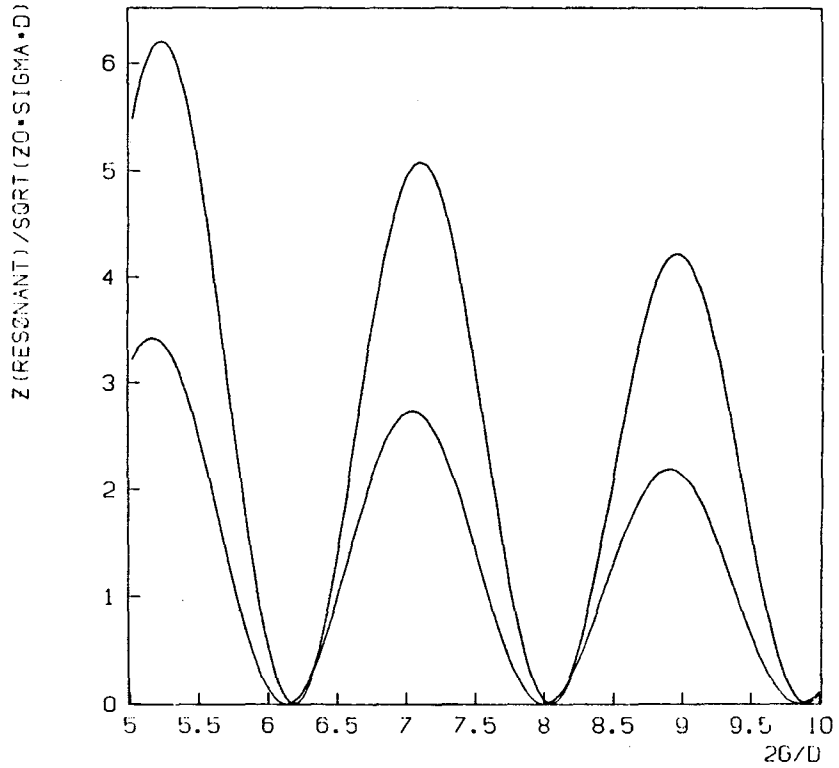

FIG. 34 BETA=.7 B/D=.4,.5

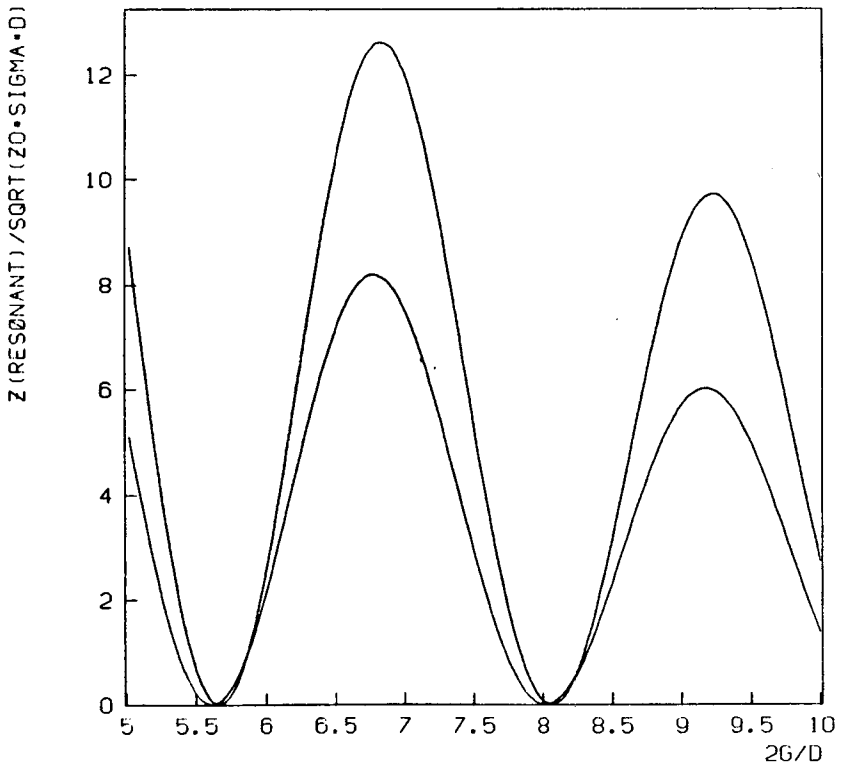

FIG.35 BETA=.9 B/D=.4,.5

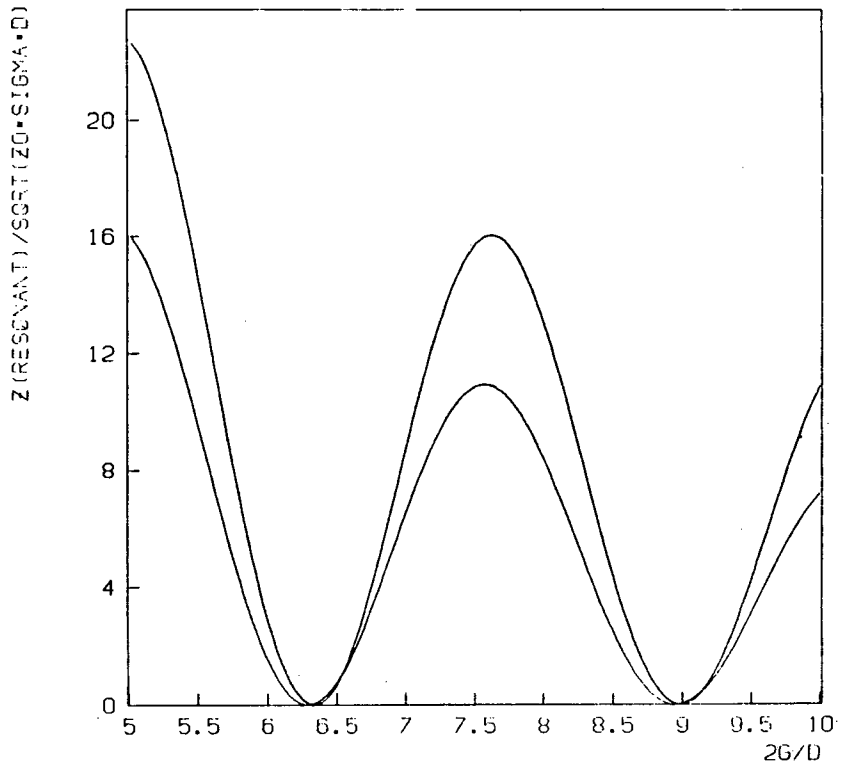

FIG.36 GAMMA=30 B/D=.4,.5

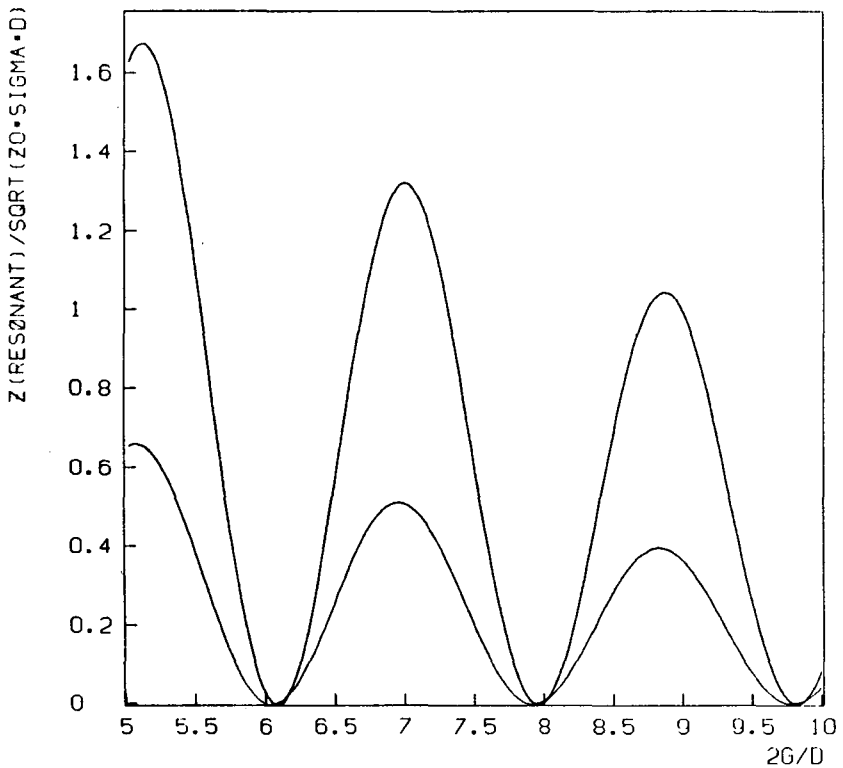

FIG.37 BETA=.7 B/D=.6,.7

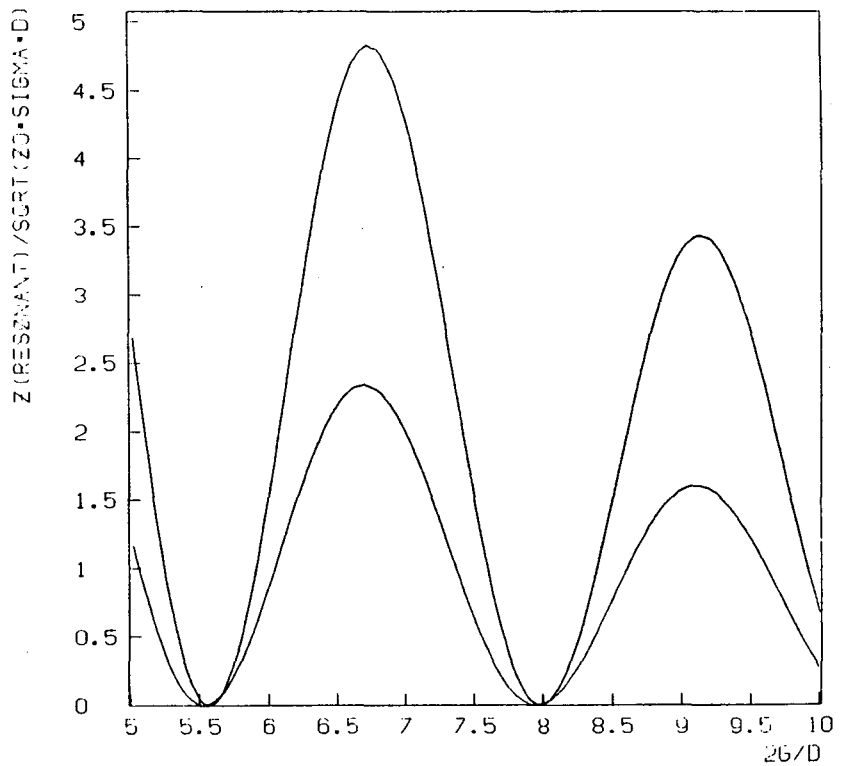

FIG.38 BETA=.9 B/D=.6,.7

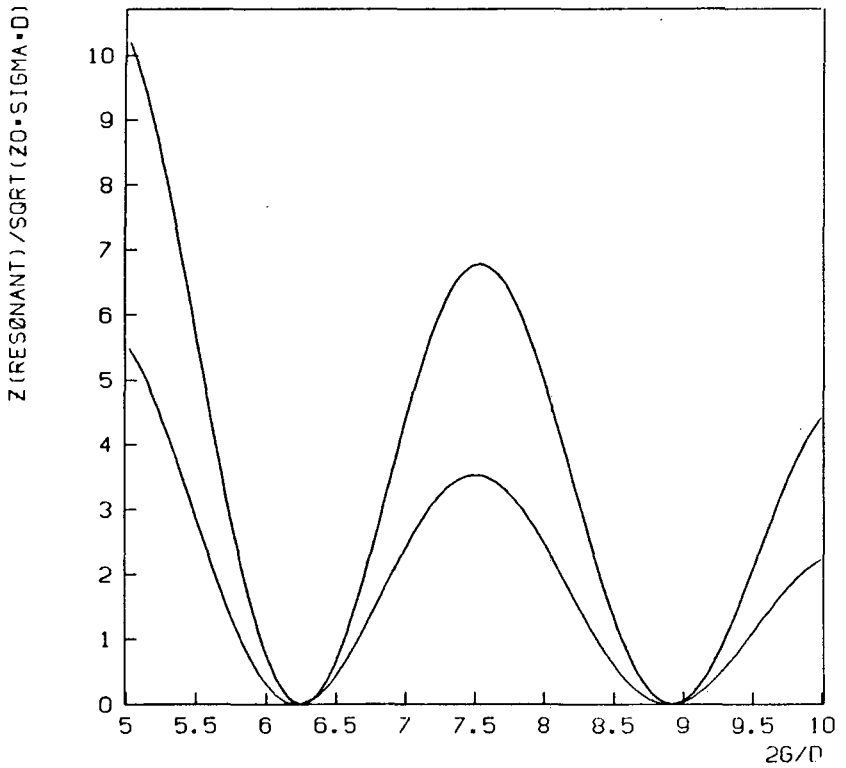

FIG.39 GAMMA=30 B/D=.6,.7

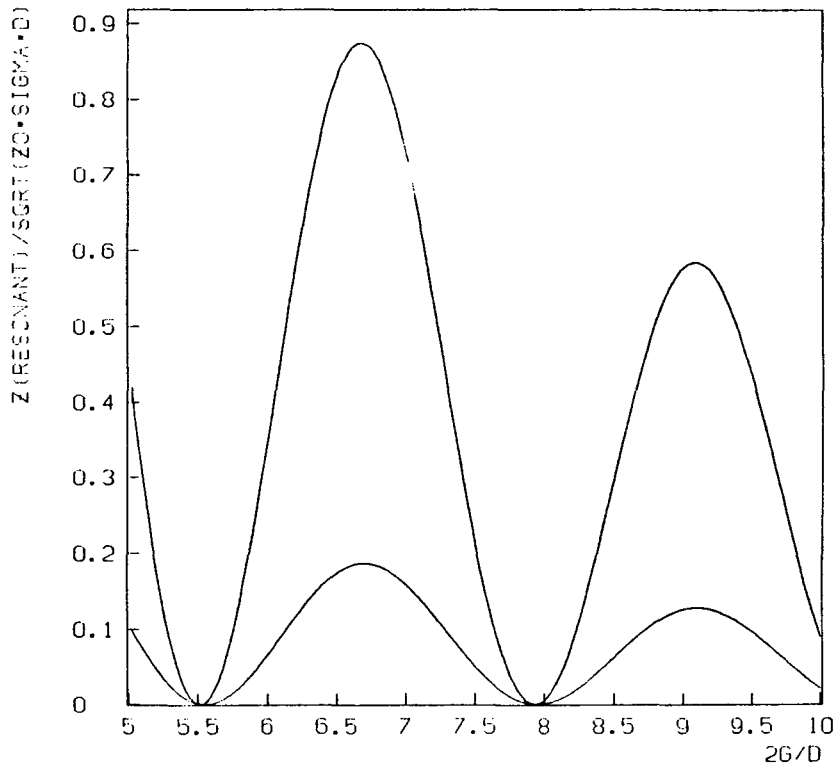

FIG.40 BETA=.9 B/D=.8,.9

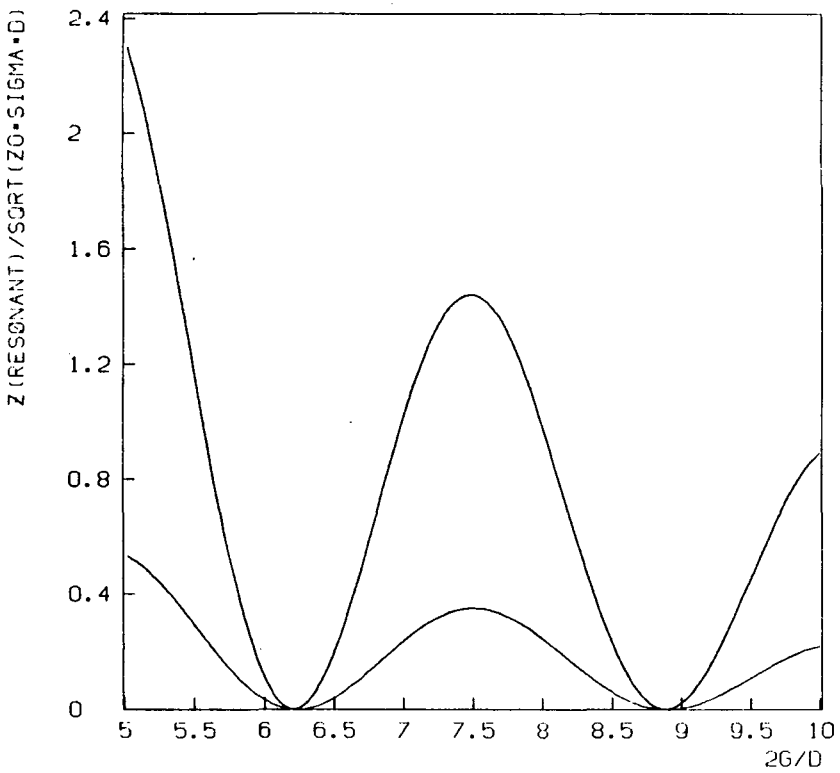

FIG.41 GAMMA=30 B/D=.8,.9

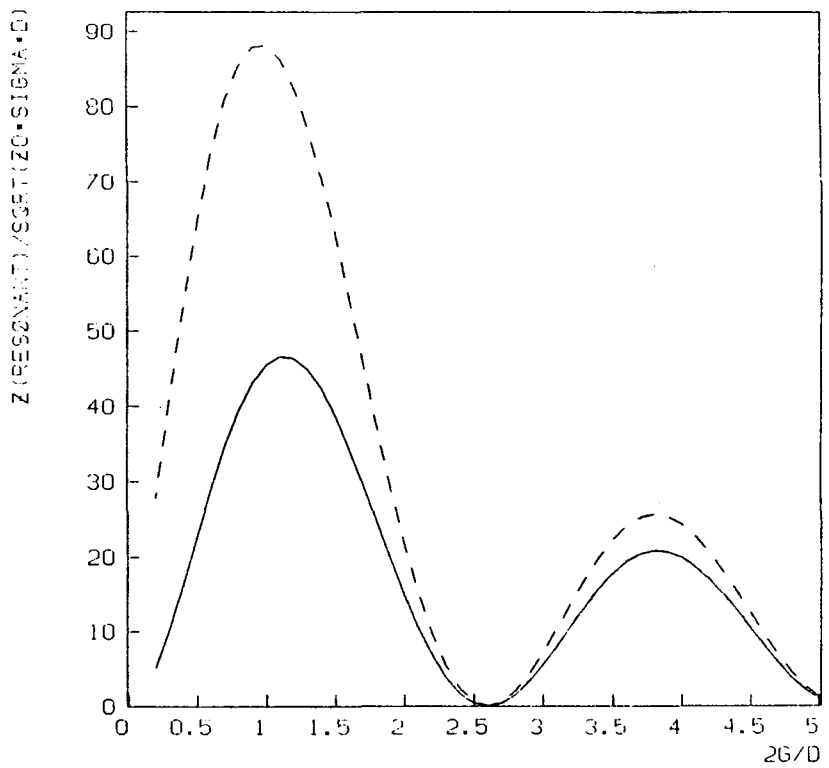

FIG.42 GAMMA=30 B/D=.3

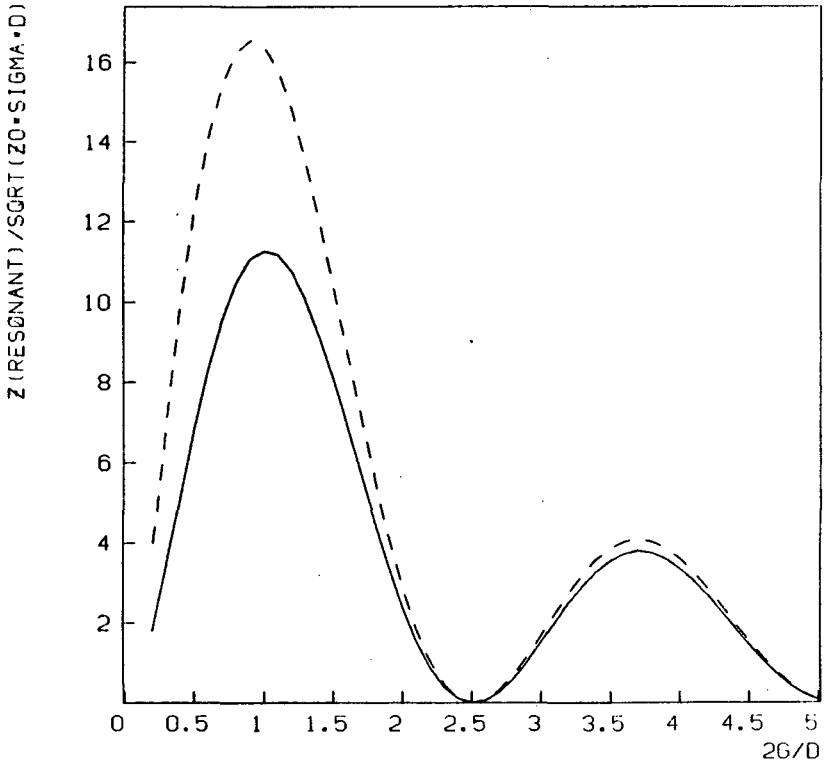

FIG.43 GAMMA=30 B/D=.7

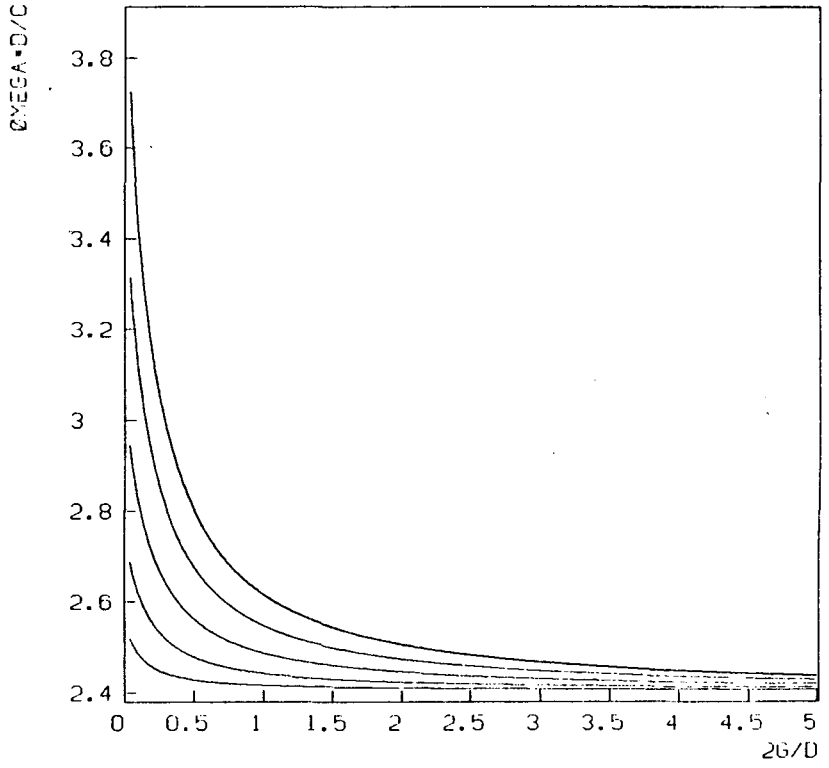

FIG.44

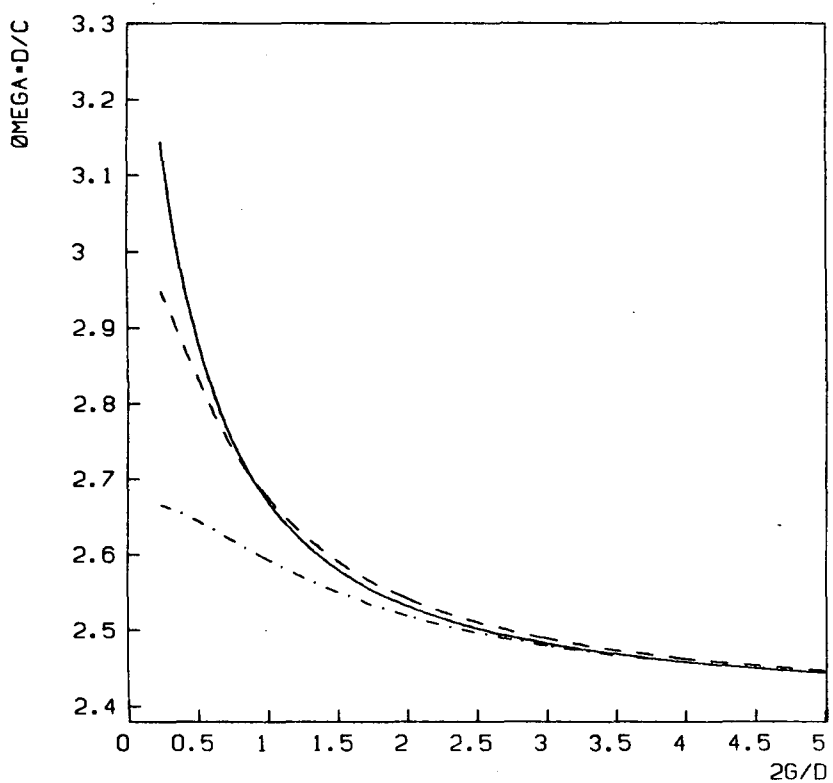
ØMEGA*D/C
3.3
3.2
3.1
3
2.9
2.8
2.7
2.6
2.5
2.4
0
0.5
1
1.5
2
2.5
3
3.5
4
4.5
5
2G/D

FIG.45

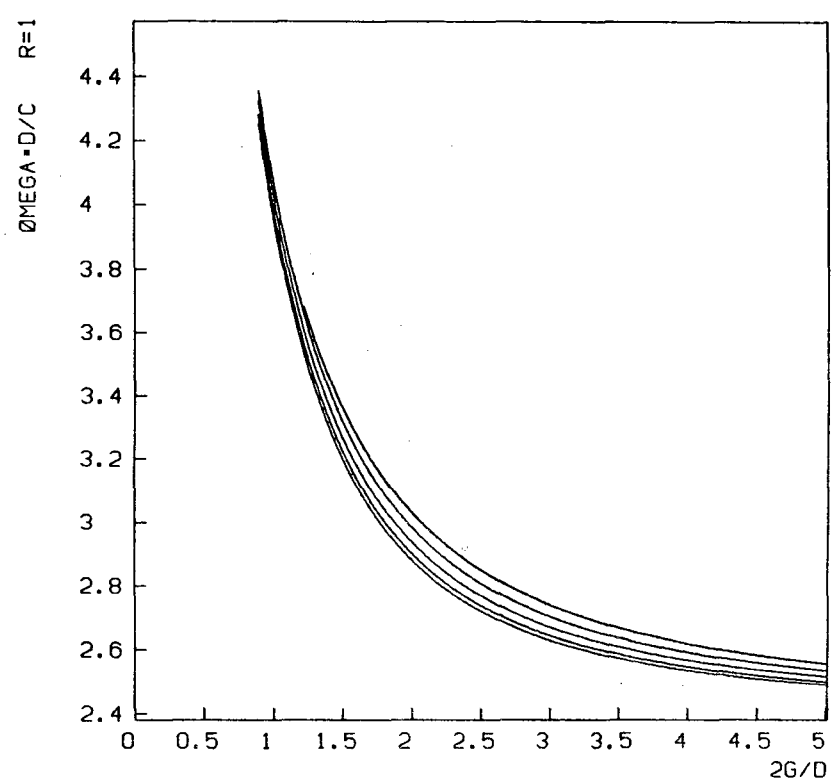
ØMEGA*D/C R=1
4.4
4.2
4
3.8
3.6
3.4
3.2
3
2.8
2.6
2.4
0
0.5
1
1.5
2
2.5
3
3.5
4
4.5
5
2G/D

FIG.46

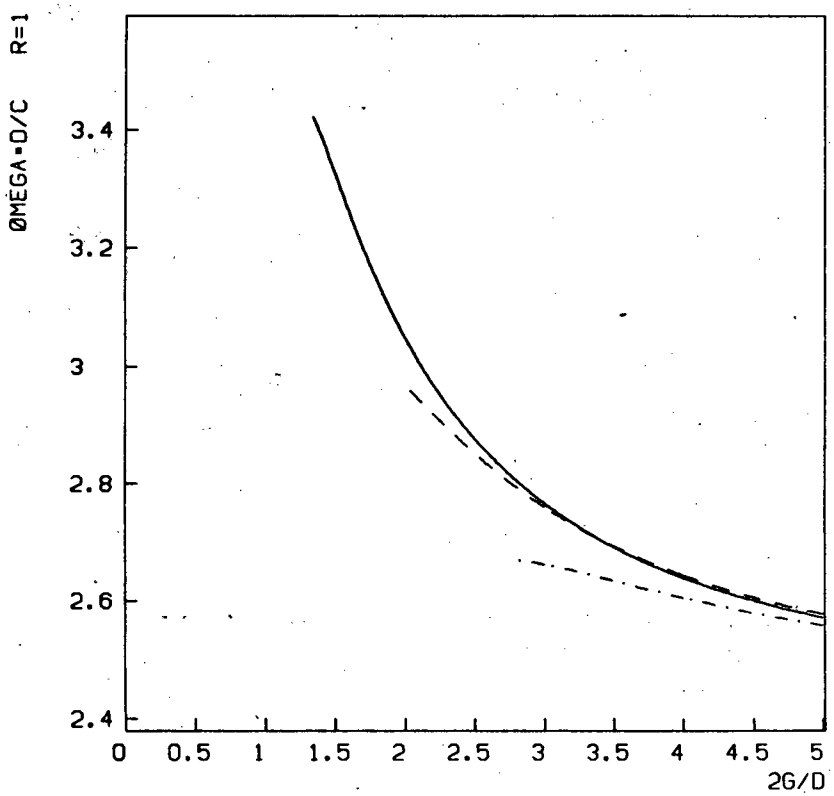
ØMEGA*D/C R=1
3.4
3.2
3
2.8
2.6
2.4
0
0.5
1
1.5
2
2.5
3
3.5
4
4.5
5
2G/D

FIG.47

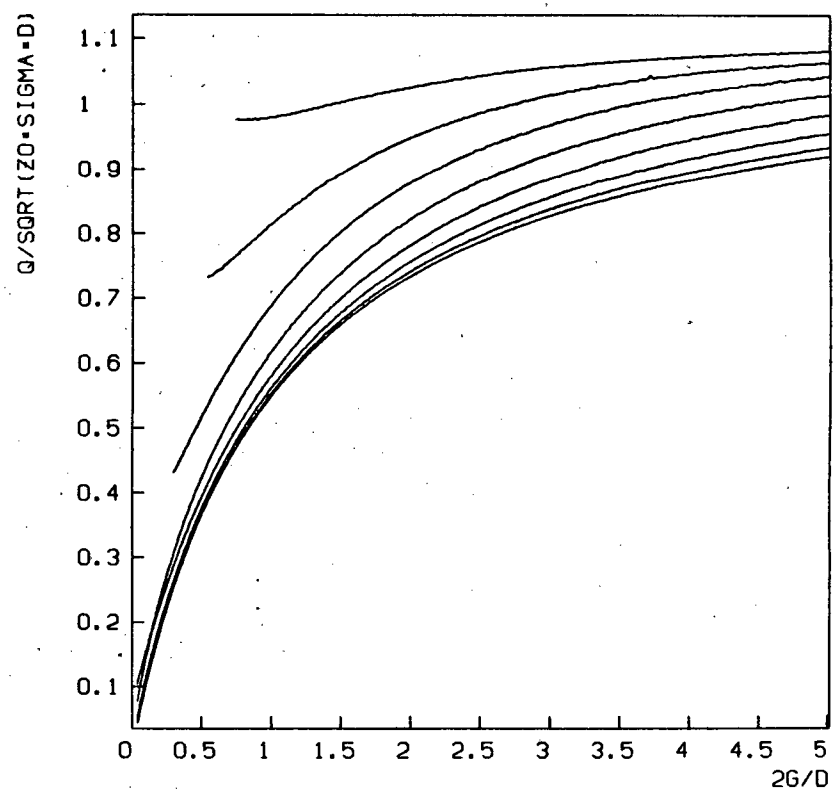
Q/SQRT(ZO*SIGMA*D)
1.1
1
0.9
0.8
0.7
0.6
0.5
0.4
0.3
0.2
0.1
0
0.5
1
1.5
2
2.5
3
3.5
4
4.5
5
2G/D

FIG.48

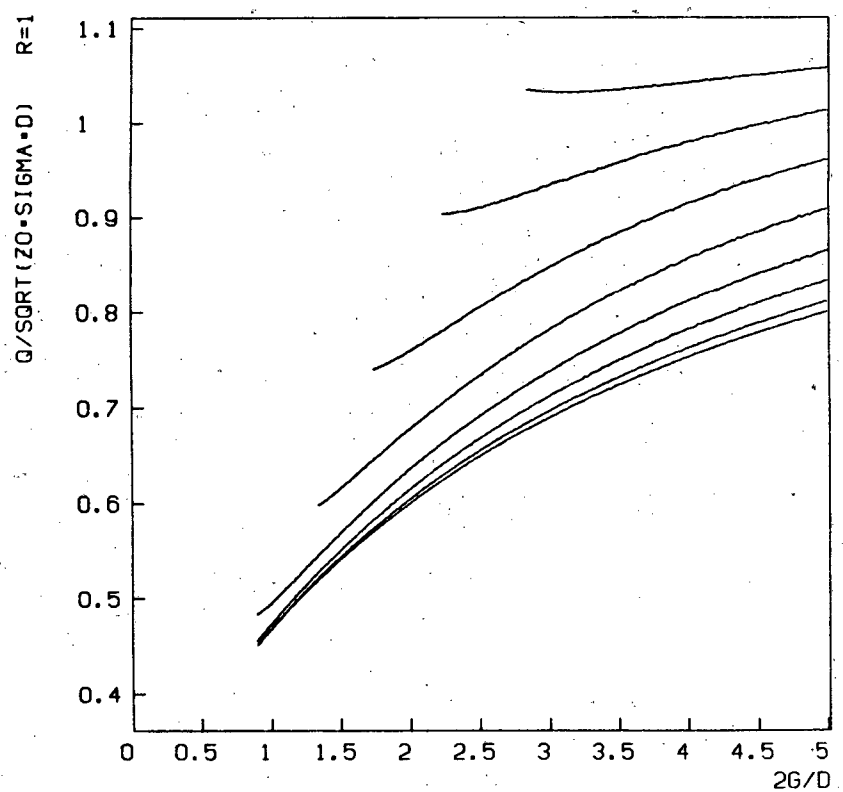
Q/SQRT(ZO•SIGMA•D) R=1
1.1
1
0.9
0.8
0.7
0.6
0.5
0.4
0
0.5
1
1.5
2
2.5
3
3.5
4
4.5
5
2G/D

FIG.49

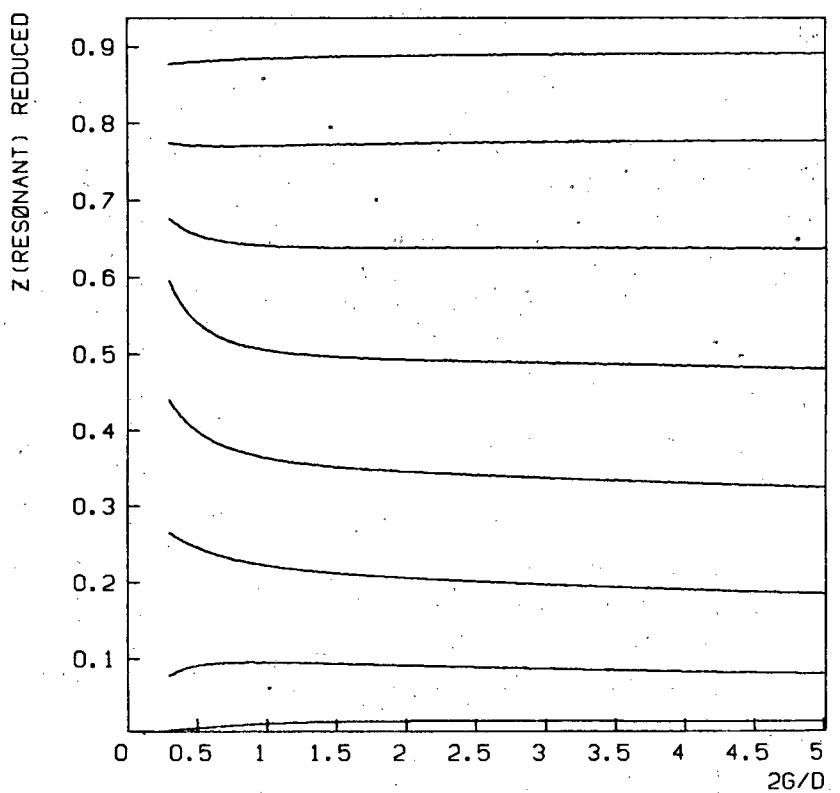
Z(RESØNANT) REDUCED
0.9
0.8
0.7
0.6
0.5
0.4
0.3
0.2
0.1
0
0.5
1
1.5
2
2.5
3
3.5
4
4.5
5
2G/D

FIG.50

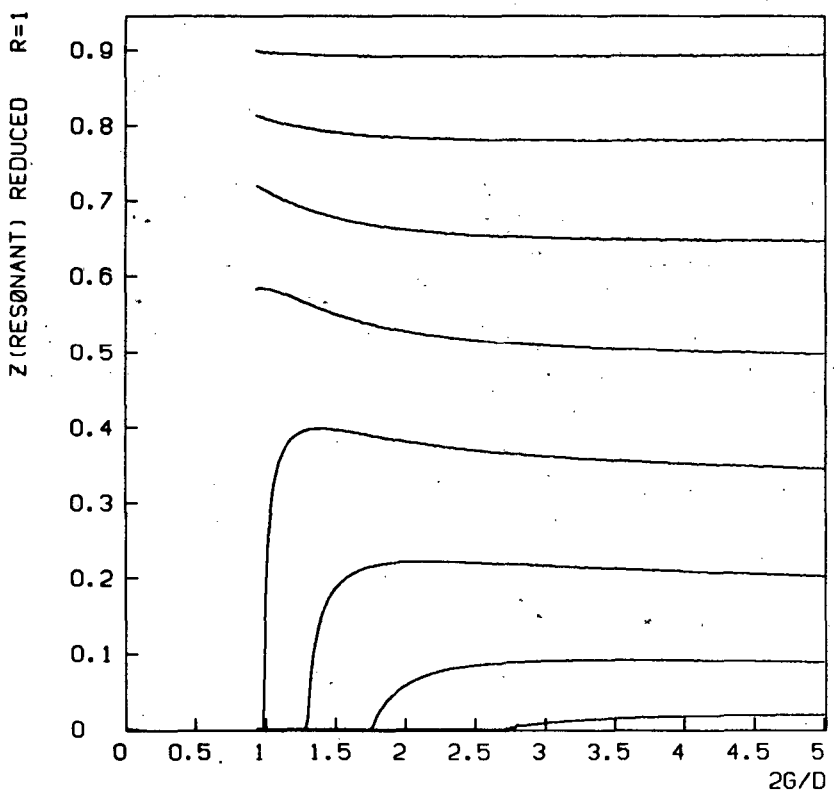

FIG.51

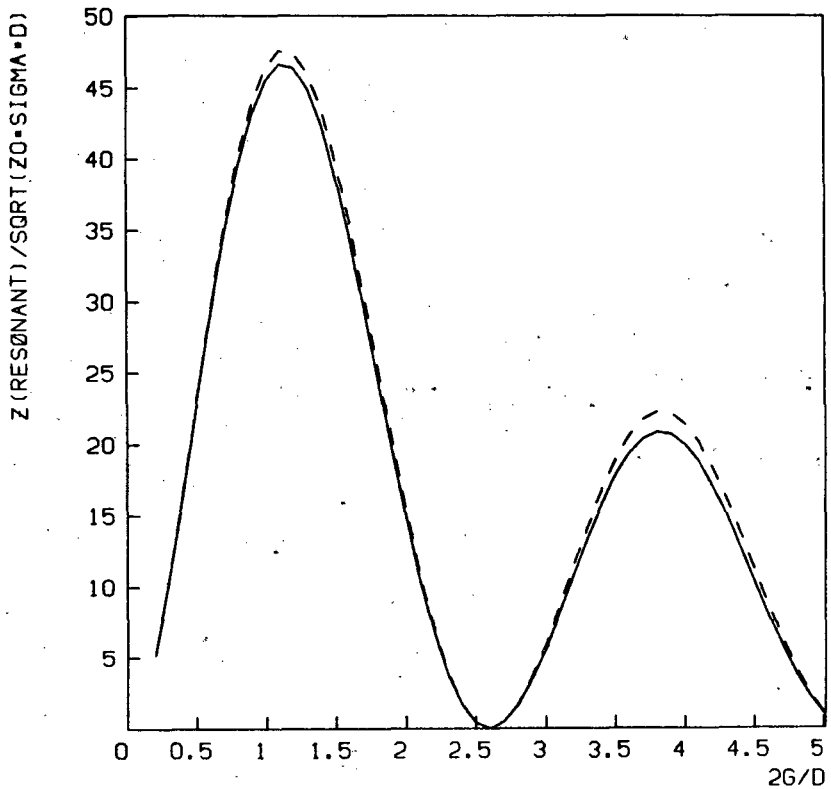

FIG.52 GAMMA=30 B/D=.3

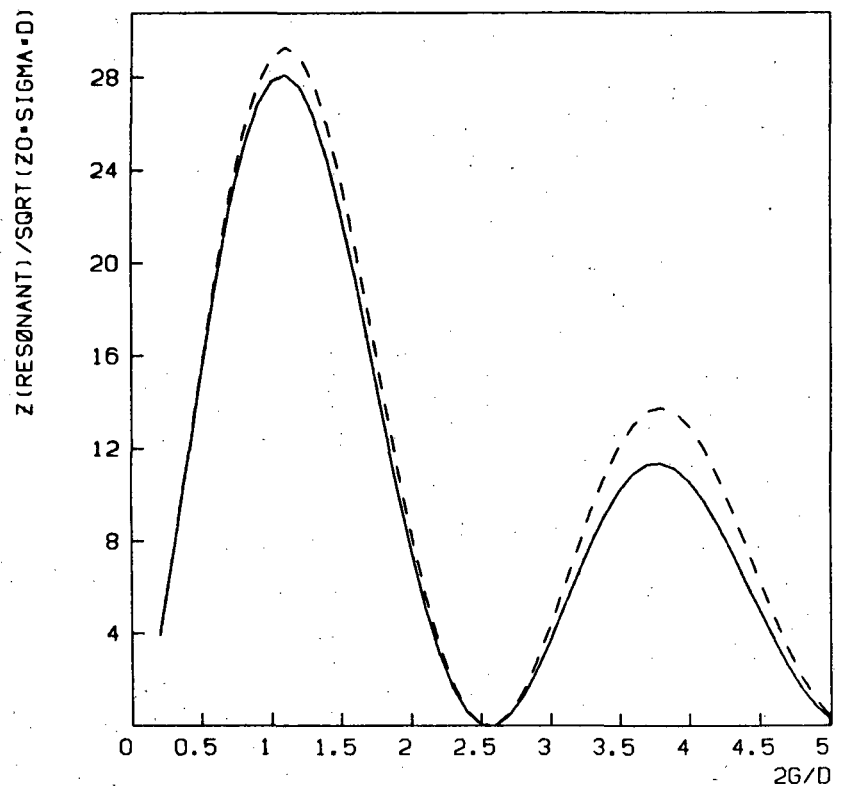

FIG.53 GAMMA=30 B/D=.5

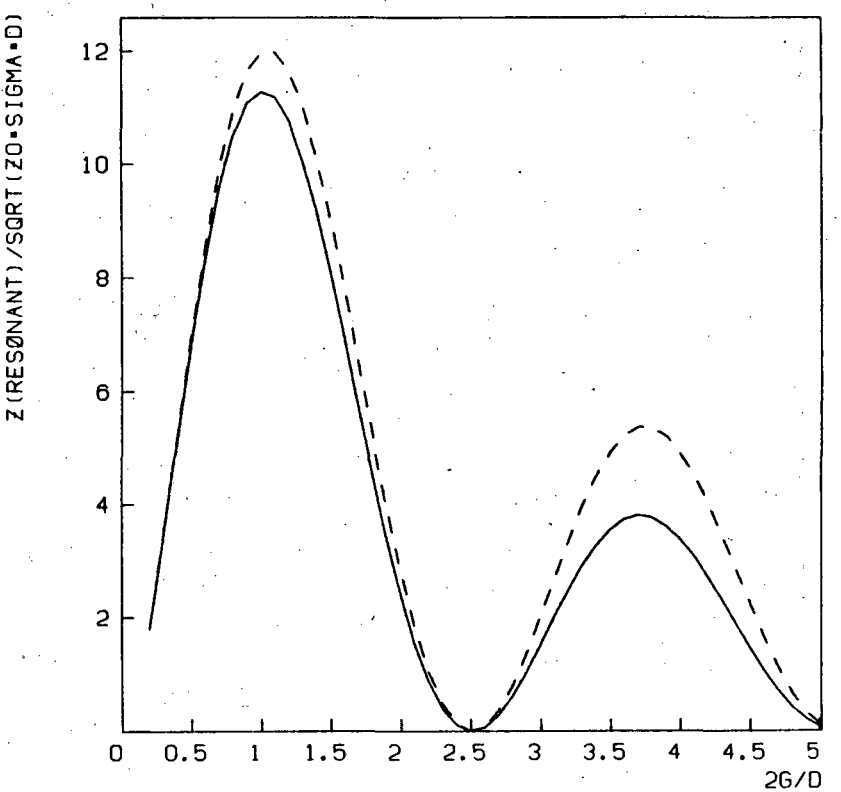

FIG.54 GAMMA=30 B/D=.7

This report was done with support from the Department of Energy. Any conclusions or opinions expressed in this report represent solely those of the author(s) and not necessarily those of The Regents of the University of California, the Lawrence Berkeley Laboratory or the Department of Energy.

Reference to a company or product name does not imply approval or recommendation of the product by the University of California or the U.S. Department of Energy to the exclusion of others that may be suitable.

TECHNICAL INFORMATION DEPARTMENT
LAWRENCE BERKELEY LABORATORY
UNIVERSITY OF CALIFORNIA
BERKELEY, CALIFORNIA 94720